Voltage Clamp Limitations of Dual Whole-Cell Gap Junction Current and Voltage Recordings. I. Conductance Measurements

Richard D. Veenstra
Department of Pharmacology, State University of New York, Upstate Medical University, Syracuse, New York 13210 USA

ABSTRACT Previous correction methods for series access resistance errors in the dual whole-cell configuration did not take into account the effect of nonzero resting potentials (E_{rest}) and junctional reversal potentials (E_{rev}). Dual whole-cell currents were modeled according to resistor-circuit analysis and two correction formulas for the measurement of junctional currents (I_j) were assessed. The equations for I_j, derived from Kirchoff's law before and after baseline subtraction of the nonjunctional current, were assessed for accuracy under a variety of whole-cell patch-clamp recording conditions. Both equations accurately correct for dual whole-cell voltage-clamp errors provided that the cellular parameters are included in the nonbaseline subtracted I_j derivations. Junctional conductance (g_j) estimates are most reliable at high junctional resistance (R_j) values and minimize the need for corrective methods based on electrode series and cellular input resistances (R_{el} and R_{in}). In the "open-cell" configuration, low R_j values relative to R_{in} are required for accurate g_j estimates. These methods provide the basis for accurate quantitative measurements of junctional resistance (or conductance) of gap junction channels or connexin hemichannels in the dual whole-cell or open-cell configurations. Revaluation of V_j-dependent gating of rat connexin40 g_j produced nearly identical Boltzmann fits to previously published data. Continuous g_j–V_j curves generated by variable slope V_j ramps provide for more accurate fits and assessment of the time-dependence of the half-inactivation voltage and net gating charge movement.

INTRODUCTION

The dual whole-cell recording configuration, where two cells are independently voltage clamped by their own whole-cell patch electrode, is routinely applied to the measurement of junctional conductance (Veenstra, 1996). Most junctional current recordings are obtained for the primary purpose of measuring the macroscopic junctional current (I_j) or resistance (R_j) in response to experimental variables that modify channel gating (Kolb and Somogyi, 1991; Veenstra, 1991a). Although the development of the patch-clamp technique made it possible to voltage clamp individual ion channels with a single electrode (Hamill et al., 1981), the nature and location of the gap junction channel precludes the direct patch approach to this plasmalemmal intercellular channel. Occasionally, small cells with high input resistances (R_{in}) expressing relatively few gap junction channels when paired permit the resolution of single-gap junction channel currents (i_j) (Neyton and Trautmann, 1985; Veenstra and DeHaan, 1986; Rook et al., 1988). Corrective measures for patch electrode series access resistance (R_{el}) errors are rarely required for i_j recordings, but become increasingly important as junctional conductance ($g_j = 1/R_j$) increases (Weingart, 1986). Two correction methods, one derived from voltage clamp analysis of a dual whole-cell resistor circuit (Veenstra and Brink, 1992), and another that modeled whole-cell currents using Kirchoff's law (Van Rijen et al., 1998), published slightly different equations that permit off-line analysis of I_j and R_j. Both methods require knowledge of R_{el} and R_{in} for each cell and subtraction of nonjunctional membrane currents (I_{in}) from the whole-cell current to obtain the value of I_j. This is best accomplished in a nonvoltage pulsed cell, because I_{in} will remain relatively constant provided that R_{in} remains stable. However, these previous derivations always assumed the voltage of the nonpulsed cell (cell 2 or the post-junctional cell) was 0 mV. When the dual whole-cell patch clamp technique is applied to living cells in primary or established cell cultures, the cellular resting potential (E_{rest}) should be considered, because setting the holding potential equal to E_{rest} will minimize unwanted nonjunctional membrane currents and improve the resolution of I_j. Furthermore, any asymmetry in E_{rest} or the whole-cell recording conditions of both cells produces small discrepancies in the initial recording conditions that must be corrected for in the experimental I_j and R_j measurements. In this manuscript, correction methods for I_j and R_j measurements are developed that more accurately reflect actual recording conditions and the effects of intrinsic cellular properties (e.g., E_{rest} or cellular membrane resistance, R_m) modified by the establishment of the dual whole-cell patch electrode configuration. Asymmetric junctional properties such as heterotypic gap junction channels, bi-ionic potentials, or unequal whole-cell voltage clamp conditions are also considered in the derivations.

The transjunctional voltage (V_j) gating of the rat connexin40 (rCx40) gap junction was reevaluated using continuous I_j–V_j relations in conjunction with I_j correction procedures, and the results are presented. Slow V_j ramps (200 ms/mV) produced half-inactivation voltage ($V_{1/2}$) and

Received for publication 5 October 2000 and in final form 15 February 2001.

Address reprint requests to Richard D. Veenstra, Dept. of Pharmacology, SUNY Upstate Medical University, 750 East Adams St., Syracuse, NY 13210. Tel.: 315-464-5145; Fax: 315-464-8014; E-mail: veenstra@mail.upstate.edu.

0006-3495/01/05/2231/17 $2.00

gating charge valence (z) values that agreed closely with previous results using conventional voltage pulse protocols. The time-dependence of $V_{1/2}$ and z were ascertained using a family of V_j ramps with different ramp speeds (ms/mV). Correction for reductions in V_j and I_j due to series resistance errors produced a slight reduction in the measured V_j-insensitive normalized g_j (G_{min}) from 0.30 to 0.23. Using a continuous G_j–V_j curve from fewer experiments than required using voltage pulse protocols reduced the variability of the fitted Boltzmann parameters.

METHODS

Figure 1 is a resistor circuit (A) and current vector diagram (B) for the dual whole-cell configuration. Each cell has its own resting potential (E_{rest}) determined by $I_{rest} \cdot R_m$ prior to establishment of the whole-cell patch electrode configuration. After GΩ seal (R_s) formation and membrane patch disruption, E_{rest} equals $I_{rest} \cdot R_{in}$ where $R_{in} = (R_m \cdot R_s)/(R_m + R_s)$. A defined current value (I_{rest}) was used instead of a defined E_{rest} to model the shunting of the resting membrane potential by a whole-cell patch electrode. It is true that $I_m = 0$ at E_{rest}, but this is because the inward and outward membrane ionic currents exactly balance each other. Because the Nernst potentials for K^+, Na^+, etc. are not changed and there is a finite resting g_{Na}, g_K, etc., the current values at which this dynamic balance is achieved is fixed for a resting membrane.

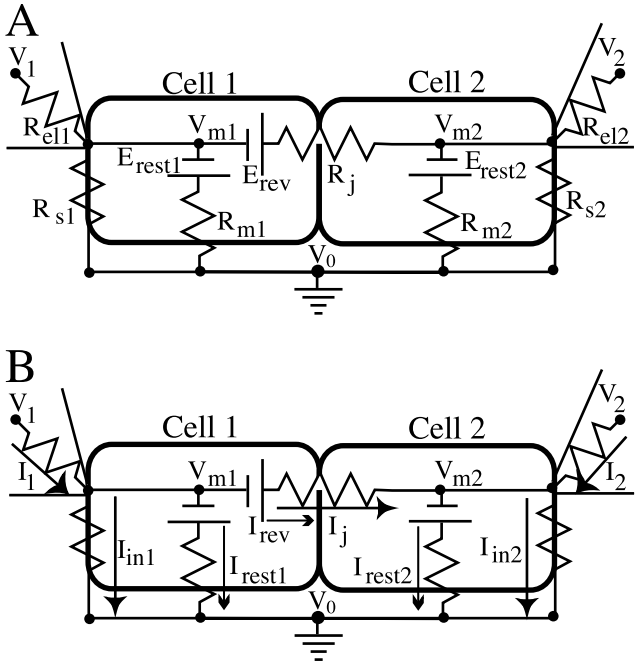

FIGURE 1 Equivalent resistive circuit for the dual whole-cell configuration. (A) Equivalent resistive circuit for a dual whole-cell voltage clamp using patch electrodes where the seal resistance, R_s, is in parallel with the membrane resistance, R_m, of each cell. A command voltage, V, is applied to cells 1 and 2 independently via patch clamp amplifiers and the membrane potential, V_m, of each cell is equal to ($V - I \cdot R_{el}$). The resting potential, E_{rest}, of each cell, determined initially by $I_m \cdot R_m$, becomes $I_m \cdot R_{in}$ in the whole-cell configuration. Any source of asymmetry (connexin or ionic composition) between the two cells can produce a voltage difference, E_{rev}, across the junctional resistance, R_j. When $V_1 = V_2$ and $R_{el1}/R_{in1} \cong R_{el2}/R_{in2}$, $V_{m1} = V_{m2}$ and the net transjunctional potential, V_j, and current, I_j, equal zero, provided that $E_{rev} = 0$. (B) The resulting current vectors in response to a $V_1 + \Delta V_1$, V_2, E_{rev}, E_{rest1}, and E_{rest2} applied to the dual whole cell resistor circuit diagrammed in panel A. A net $V_j \cong \Delta V_1$ and I_j proportional to $-\Delta I_2$ (see Eqs. 1g and 1i) are produced, and the exact value of $R_j = V_j/I_j$ can be determined by the net $\Delta V_1/I_j$. I_{rev} is a DC component of I_j, and I_{rest} is a DC component of I_{in} for each cell.

Each patch electrode has a resistance (R_{el}) in series with R_{in} and R_j that will affect those measured values. The command potentials of each patch electrode (V_1 and V_2) initially begin with $V_1 = V_2$ followed by alteration of one command potential (ΔV) to impose a voltage gradient across R_j and determine the value of I_j from the resultant whole-cell currents (I_1 and I_2). To evaluate the model circuit, a command $V_{j,comm} = V_1 - V_2$ was varied by ±100 mV in 10-mV increments. Initial values of R_{el1} and R_{el2}, R_{s1} and R_{s2}, R_{m1} and R_{m2}, R_j, and I_{rest1} and I_{rest2} were assigned, and the whole-cell voltages (V_{m1} and V_{m2}) and currents (I_1 and I_2) were calculated for each $V_{j,comm}$. Optimal recording conditions initially assigned to the dual whole-cell circuit were $R_{el} = 10\ M\Omega\ (\leq 100 \cdot R_m)$, $R_s = 10\ G\Omega\ (\geq 10 \cdot R_m)$, $R_j = 1\ G\Omega\ (\leq R_m)$, and $R_m = 1\ G\Omega$. These values approximate dual whole-cell conditions from connexin-transfected mammalian cell lines or primary cell cultures with cell diameters of ≤20 μm. The following set of equations defines the whole-cell current and voltage values of the dual-cell circuit before and after establishment of the dual whole-cell patch electrode configuration.

Dual whole-cell voltage clamp equations

$$I_{total} = I_1 + I_2 \tag{1a}$$

$$I_1 = I_{in1} + I_j \tag{1b}$$

$$I_2 = I_{in2} - I_j \tag{1c}$$

$$V_{m1} = V_1 - (I_1 \cdot R_{el1}) \tag{2a}$$

$$V_{m2} = V_2 - (I_2 \cdot R_{el2}) \tag{2b}$$

$$E_{rest1} = I_{rest1} \cdot R_{in1} \tag{3a}$$

$$E_{rest2} = I_{rest2} \cdot R_{in2} \tag{3b}$$

To model the whole-cell currents, the following expressions were derived from the resistor circuit diagram (Fig. 1):

$$I_1 = \frac{V_{m1} - E_{rest1}}{R_{in1}} + \frac{V_{m1} - V_{m2} - E_{rev}}{R_j} = \frac{[V_1 - (I_1 \cdot R_{el1})] - E_{rest1}}{R_{in1}} + \frac{[V_1 - (I_1 \cdot R_{el1})] - [V_2 - (I_2 \cdot R_{el2})] - E_{rev}}{R_j}, \tag{4a}$$

$$I_2 = \frac{V_{m2} - E_{rest2}}{R_{in2}} - \frac{V_{m1} - V_{m2} - E_{rev}}{R_j} = \frac{[V_2 - (I_2 \cdot R_{el2})] - E_{rest2}}{R_{in1}} - \frac{[V_1 - (I_1 \cdot R_{el1})] - [V_2 - (I_2 \cdot R_{el2})] - E_{rev}}{R_j}. \tag{4b}$$

These expressions for the ideal whole-cell currents cannot be solved for I_1 and I_2 because it is not possible to solve for V_{m1} and V_{m2} without knowing the values of I_1 and I_2. To solve for I_1 and I_2 independently knowing only the initial V, I_{rest}, and R values of the model circuit, we again solve for Eqs. 1b and 1c knowing that $I = V/R_{total}$ for each current path. For each cell

$$I_{in} = \frac{V \cdot R_{in} - E_{rest} \cdot (R_{el} + R_{in})}{(R_{el} + R_{in}) \cdot R_{in}}, \tag{5}$$

and

$$I_j = \frac{\lfloor (V_1 - V_2) \cdot R_j \rfloor - \lfloor E_{rev} \cdot (R_{el1} + R_j + R_{el2}) \rfloor}{(R_{el1} + R_j + R_{el2}) \cdot R_j}. \tag{6}$$

The appropriate expressions for I_1 and I_2 become

$$I_1 = \frac{V_1 \cdot R_{in1} - E_{rest1} \cdot (R_{el1} + R_{in1})}{(R_{el1} + R_{in1}) \cdot R_{in1}} + \left[\frac{[(V_1 - V_2) \cdot R_j] - [E_{rev} \cdot (R_{el1} + R_j + R_{el2})]}{(R_{el1} + R_j + R_{el2}) \cdot R_j} \right] \tag{4c}$$

and

$$I_2 = \frac{V_2 \cdot R_{in2} - E_{rest2} \cdot (R_{el2} + R_{in2})}{(R_{el2} + R_{in2}) \cdot R_{in2}} - \left[\frac{[(V_1 - V_2) \cdot R_j] - [E_{rev} \cdot (R_{el1} + R_j + R_{el2})]}{(R_{el1} + R_j + R_{el2}) \cdot R_j} \right] \tag{4d}$$

Whole-cell junctional current and resistance equations

Experimental determination of R_j from dual whole-cell currents requires estimation of I_j and calculation of R_j according to Ohm's Law, $R_j = V_j/I_j$. R_j is experimentally determined by measuring I_j in response to an applied V_j. V_j is defined as the difference in the two command potentials V_1 and V_2. Initially $V_1 = V_2$ and a ΔV pulse is applied to one cell conventionally defined as cell 1 (prejunctional cell). One cell must be chosen as the reference for calculating V_j and if V_j is defined as $V_1 - V_2$, then $V_j = \Delta V_1$. However, R_{el} is in series with R_{in} of each cell so the actual value of

$$V_j = V_{m1} - V_{m2} = [(V_1 + \Delta V_1) - V_2] - [(R_{el1} \cdot I_1) - (R_{el2} \cdot I_2)] \tag{2c}$$

(Rook et al., 1988; Veenstra and Brink, 1992). I_j appears in both whole-cell current signals but with opposite sign (Eqs. 1b and 1c) (Veenstra and DeHaan, 1986). Expressions for I_j using either whole-cell signal were derived from Kirchoff's law where

$$I_j = I_1 \cdot \left(1 + \frac{R_{el1}}{R_{in1}}\right) - \frac{V_1}{R_{in1}} \tag{1e}$$

or

$$I_j = -I_2 \cdot \left(1 + \frac{R_{el2}}{R_{in2}}\right) + \frac{V_2}{R_{in2}} \tag{1f}$$

(Weingart, 1986; Rook et al., 1988; Eq. A8 and A9 of Van Rijen et al., 1998) because R_m measured in the whole-cell configuration is R_{in}. Because V_1 is altered by the ΔV step, $I_{in1} = [V_1 (+ \Delta V_1)]/R_{in1}$ does not remain constant. Therefore, $-I_2$ is conventionally used to measure I_j (Veenstra and DeHaan, 1986; Weingart, 1986). Veenstra and Brink (1992) derived a related expression for I_j based on resistive circuit analysis where

$$I_j = -\Delta I_2 \cdot \left(1 + \frac{R_{el2}}{R_{in2}}\right) \tag{1g}$$

(Eq. 6 in Veenstra and Brink, 1992). If one subtracts Eq. 1f when $V_1' = V_1 + \Delta V$ from the initial condition when $V_1 = V_2$, one obtains Eq. 1g because V_2 and R_{in2} (ideally) remain constant and the I_{in2} terms cancel out. This is the original definition for $I_j = -\Delta I_2$ (see Veenstra, 1991b). The condition that V_{m2} when $V_1 = V_2$ equals V_{m2} when $V_1 \neq V_2$ does not actually hold true because a small fraction of I_j must flow across R_{in2} in the whole-cell configuration, resulting in a small change in V_{m2}

$$\Delta V_{m2} = I_j \cdot \left[\frac{R_{el2} \cdot R_{in2}}{(R_{el2} + R_{in2})} \right] = I_j \cdot R_{c2} \tag{2d}$$

during the ΔV_1 step. This equation first appeared as Eq. 9 in Veenstra and Brink (1992). The cellular resistance (R_c) was defined as the input resistance of the whole-cell relative to the junction. The Kirchoff's law expressions for I_j, when the "real" cell parameters of E_{rest1} and E_{rest2} (Fig. 1) are considered become

$$I_j = I_1 \cdot \left(1 + \frac{R_{el1}}{R_{in1}}\right) - \frac{(V_1 - E_{rest1})}{R_{in1}}, \tag{1h}$$

and

$$I_j = -I_2 \cdot \left(1 + \frac{R_{el2}}{R_{in2}}\right) + \frac{(V_2 - E_{rest2})}{R_{in2}}. \tag{1i}$$

Because $R_j = V_j/I_j$, the expressions for estimating R_j from dual whole-cell voltage clamp currents are

$$R_j = \frac{[(V_1 + \Delta V_1) - V_2] - [(R_{el1} \cdot I_1) - (R_{el2} \cdot I_2)] - E_{rev}}{-I_2 \cdot (1 + (R_{el2}/R_{in2})) + ((V_2 - E_{rest2})/R_{in2})} \tag{5a}$$

or

$$R_j = \frac{[(V_1 + \Delta V_1) - V_2] - [(R_{el1} \cdot I_1) - (R_{el2} \cdot I_2)] - E_{rev}}{-\Delta I_2 \cdot (1 + (R_{el2}/R_{in2}))}. \tag{5b}$$

The major difference between these two approaches is in the estimation of I_{in2} in Eq. 5a and the subtraction of I_2 ($\cong I_{in2}$) when $V_1 = V_2$ in Eq. 5b. The uncompensated R_j estimate for the purpose of evaluating the correction methods was defined as

$$R_j = \frac{V_1 - V_2}{-\Delta I_2}, \tag{5c}$$

where

$$V_j = V_1 - V_2 \tag{2e}$$

and

$$I_j = -\Delta I_2. \tag{1j}$$

RESULTS

Experimental determination of R_{el} and R_{in}

The whole-cell capacitive transient decay time constant in response to a small voltage step ($\Delta V_1 = \Delta V_2$) is used to determine the value of R_{el} according to

$$\tau_{cap} = R_{el} \cdot C_{in} \tag{6}$$

(Hamill et al., 1981; Sakmann and Neher, 1995). This measurement also requires integration of the cellular input capacitance (C_{in}) for each cell from the total charge (Q_{in}) of the whole-cell capacitive transient according to Faraday's law ($C_{in} = Q_{in}/\Delta V$). R_{in1} and R_{in2} are assessed experimentally by varying $V_1 = V_2$ simultaneously to minimize I_j ($V_j \cong 0$ mV). ΔV can be a single step or a voltage ramp or staircase that determines R_{in} over a range of voltages (e.g., -100 to $+60$ mV, physiological voltage range). This experimental determination of R_{in} ignores any preexisting V_j due to $E_{rest1} \neq E_{rest2}$, $V_{m1} \neq V_{m2}$, or $E_{rev} \neq 0$ mV. For example, if $I_1 \cdot R_{el1} \neq I_2 \cdot R_{el2}$ even when $V_1 = V_2$, $E_{rest1} = E_{rest2}$, and $E_{rev} = 0$, then $V_{m1} \neq V_{m2}$ (Eqs. 2a and 2b) and $I_j \neq 0$ (Eqs. 1g and 1i). In actual terms, $V_{m1} = V_{m2}$ only when $V_1 = V_2$, $(R_{el1}/R_{in1}) = (R_{el2}/R_{in2})$, and $(V_1 - E_{rest1}) = (V_2 - E_{rest2})$. So minor asymmetries in the dual whole-cell circuit will result in $V_j \neq 0$ when $V_1 = V_2$. These minor differences are often negligible (<1 mV).

Experimental determination of E_{rest}

By definition, $E_{rest1} = V_1$ when $I_1 = 0$ and $V_1 = V_2$ (and $E_{rest2} = V_2$ when $I_2 = 0$). However, Eq. 1b infers that $I_1 = 0$ only when $I_{in2} + I_j = 0$ (or $I_2 = 0$ when $I_{in2} - I_j = 0$, Eq. 1c). Therefore, any asymmetries in R_{el}/R_{in} and $V - E_{rest}$ will produce errors in the actual E_{rest1} and E_{rest2} measurements. These errors are typically small unless R_{in} is low or R_{el} is high and can be essentially ignored. Precise determination of E_{rest} requires determining the applied V where $I = 0$ and solving Eqs. 4c and 4d for E_{rest},

$$E_{rest1} = \left[\frac{V_1}{R_{el1} + R_{in1}} - \frac{(V_{m1} - V_{m2} - E_{rev})}{R_j}\right] \cdot R_{in1}, \tag{7a}$$

and

$$E_{rest2} = \left[\frac{V_2}{R_{el2} + R_{in2}} + \frac{(V_{m1} - V_{m2} - E_{rev})}{R_j}\right] \cdot R_{in2}. \tag{7b}$$

A nonzero E_{rev} can develop from an asymmetric (heterotypic) gap junction channel or asymmetric ionic conditions in addition to unequal dual whole-cell parameters. The condition of $E_{rev} \neq 0$ will be considered in another manuscript on the subject of experimental E_{rev} measurements. Eqs. 7a and 7b are not practical when R_j is unknown, as in a biological dual whole-cell experiment when $V_{m1} \neq V_{m2}$. Because $[(V_{m1} - V_{m2})/R_j]$ equals I_j, the E_{rest} measurements when $I_1 = 0$ and $I_2 = 0$ will be in error. However, when $I_1 + I_2 = 0$ the unknown I_j term cancels out and the solution to Eqs. 4c + 4d = 0 becomes

$$\frac{E_{rest1}}{R_{in1}} + \frac{E_{rest2}}{R_{in2}} = V \cdot \left[\frac{1}{R_{el1} + R_{in1}} + \frac{1}{R_{el2} + R_{in2}}\right]. \tag{8a}$$

Eq. 8 can be solved from the whole-cell input resistance and capacitance current signals required to make any series resistance corrections of dual whole-cell I_j or R_j measurements. It is apparent that

$$E_{rest} = \frac{V \cdot R_{in}}{R_{el} + R_{in}} \tag{8b}$$

for each cell. In general terms, $E_{rest} = V$ provided that $E_{rev} = 0$ and $V_{m1} = V_{m2}$.

Dual whole-cell recording conditions

To evaluate the accuracy of the three experimental R_j estimates (Eqs. 5a–c) under a variety of dual whole-cell voltage clamp conditions, R_{el}, R_{in}, and E_{rest} were altered from initial optimal dual whole-cell conditions. Whole-cell currents were modeled using Eqs. 4c and 4d and the I_j and R_j estimates using Eqs. 1g and 1i, and Eqs. 5a–c were calculated for each set of experimental conditions. The whole-cell parameters that were altered for each set of experimental conditions are listed in Table 1. Cellular parameters that remained constant were $R_{m1} = R_{m2} = 1$ GΩ and $E_{rev} = 0$

TABLE 1 Resistor and voltage values for dual whole-cell experiments

Experimental Condition	R_{el1} (MΩ)	R_{el2} (MΩ)	R_{s1} (GΩ)	R_{s2} (GΩ)	R_{in1}* (GΩ)	R_{in2}* (GΩ)	E_{rest1}† (mV)	E_{rest2}† (mV)
Optimal	10	10	10	10	0.91	0.91	−36.4	−36.4
High R_{el}	20	20	10	10	0.91	0.91	−36.4	−36.4
Low R_{in}	10	10	1	1	0.50	0.50	−20	−20
$V \neq E_{rest}$	10	10	10	10	0.91	0.91	−72.7	−72.7
Realistic	25	20	10	10	1.30‡	1.67§	−34.8‡	−33.3§

*$R_{in} = (R_s \cdot R_m)/(R_s + R_m)$.
†$E_{rest} = I_{rest} \cdot R_{in}$. I_{rest} was −40 or −80 pA.
‡$R_{in1} = 1.30$ GΩ because R_{m1} was increased to 1.5 GΩ. I_{rest1} was reduced to −26.7 pA.
§$R_{in2} = 1.67$ GΩ because R_{m2} was increased to 2.0 GΩ. I_{rest2} was reduced to −20 pA.

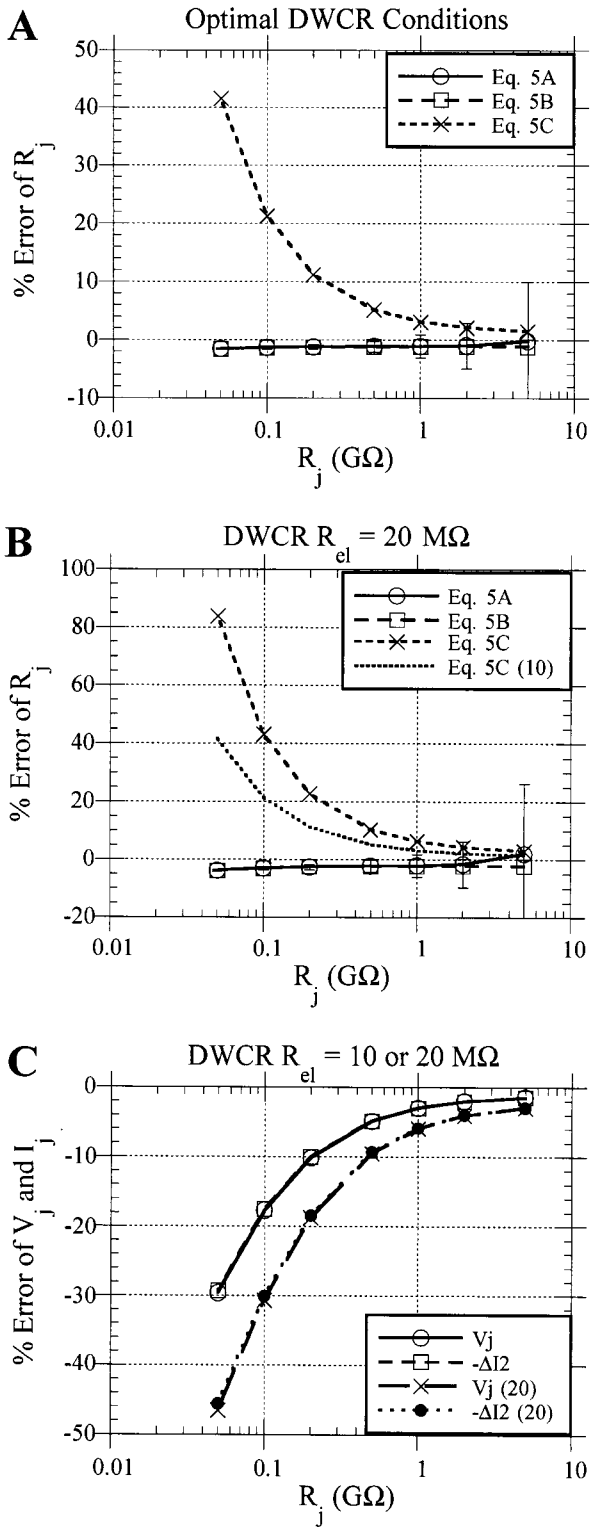

FIGURE 2 R_j, V_j, and I_j measurements under optimal dual whole-cell conditions. (*A*) The estimated R_j values from Eqs. 5a–c were determined at the specified R_j values of 0.05, 0.10, 0.20, 0.50, 1.0, 2.0, and 5.0 GΩ, and the percent error of the estimated value was plotted accordingly. Eqs. 5a and 5b provide only slightly different R_j estimates due to different definitions of $I_j = -\Delta I_2 \cdot [1 + (R_{el2}/R_{in2})]$ or $-I_2 \cdot [1 + (R_{el2}/R_{in2})] + I_{in2}$, respectively. Eq. 5c represents an uncompensated R_j estimate based only on the values of $(V_1 - V_2)$ and $-\Delta I_2$. Optimal dual whole-cell recording (DWCR) conditions of $R_{el1} = R_{el2} = 1\%$ of $R_{m1} = R_{m2}$ and $R_{s1} = R_{s2} = 10 \cdot R_m$, where $R_m = 1$ GΩ were used for these calculations (see Table 1). The common holding potential ($V_1 = V_2$) was −40 mV, $E_{rev} = 0$ mV, and $E_{rest1} = E_{rest2} = -36.4$ mV in the whole-cell configuration because $R_{in1} = R_{in2} = 0.91$ GΩ and $I_{rest1} = I_{rest2} = -40$ pA. (*B*) The same as in part A except that $R_{el1} = R_{el2} = 2\%$ of $R_{m1} = R_{m2}$. The percent error increases for all three R_j estimates, but the percent error remains <5% for all values of R_j according to Eq. 5a and 5b. The percent error in the uncompensated R_j estimate rises rapidly and exceeds 10% for $R_j > 1$ GΩ. (*C*) The percent error in the V_j and I_j estimates according to Eq. 2c and 1g or 1i. The I_j estimates using Eq. 1g and 1i were identical for $R_j < 1$ GΩ and varied slightly from each other at higher R_j values.

mV. For each set of experimental recording conditions, a series of R_j values were used to determine the accuracy of the different R_j estimation methods. Representative R_j values were 5, 2, and 1 GΩ, and 500, 200, 100, and 50 MΩ. These values were chosen because they represent reasonable experimental g_j values ranging from a 200-pS channel to a 20-nS cell pair.

Optimal dual whole-cell conditions

Bilateral symmetry and a common holding potential near the intrinsic resting potential ($V \cong E_{rest}$) characterize the optimal dual whole-cell experiment. The actual $E_{rest1} = E_{rest2} = -36.4$ mV instead of the −40-mV value of the intact cell because an R_s of $10 \cdot R_m$ yields a $R_{in} = 0.91 \cdot R_m$. This produces a small holding current (I_{in}) of −3.5 pA at the common holding potential of −40 mV. Figure 2 *A* illustrates the percent error in the R_j estimate obtained with Eqs. 5a, b, and c. Because the modeled whole-cell currents already account for series resistance errors due to R_{el}/R_{in}, the $[1 + (R_{el}/R_{in})]$ term was omitted from the I_j estimates for Eqs. 5a and 5b. To model the attenuation expected from the whole-cell circuit, the $-\Delta I_2$ term was divided by the $[1 + (R_{el}/R_{in})]$ term for Eq. 5c. The results of Eqs. 5a and 5b vary only slightly with R_j increasing to a maximum error of −1.5% at $R_j = 50$ MΩ ($g_j = 20$ nS) while an uncompensated R_j estimate (Eq. 5c) rises to an error of +41% under the identical conditions. The major source of error is the drop in the actual V_j of up to −30% due to the increasing $I_j \cdot R_{el}$ as R_j decreased. The uncompensated value of $-\Delta I_2$ closely matched (within 1%) the percent error in the applied V_j at all R_j values (Fig. 2 *C*). The small difference in the percent error between $-\Delta I_2$ and V_j equals the R_{el1}/R_{in1} attenuation factor of 1.1%.

Series resistance factors

Because the R_{el1}/R_{in1} ratio only increases the error in the current signal by 1% for every 10 MΩ/GΩ, doubling R_{el1} and R_{el2} has only modest effects on the compensated R_j estimates, whereas the percent error in the uncompensated

R_j estimate doubles (Fig. 2 *B*). Again, the major source of error is the decrease in actual V_j due to the voltage drops across each electrode (Fig. 2 *C*). As I_j increased, the percent error in R_j using either Eqs. 5a or 5b increased to only -3.8% at $g_j = 20$ nS compared to $+83\%$ using Eq. 5c. Hence, calculating V_{m1} and V_{m2} using Eqs. 2a and 2b can significantly enhance the accuracy of R_j estimates. The simple correction of using $V_j = V_{m1} - V_{m2}$ instead of $V_j = V_1 - V_2$ will account for most (>90%) of the error in the R_j estimate except under the worst circumstances ($R_{el} > 10\%$ of R_{in}).

Nonjunctional current considerations

Lowering R_{in} There are two ways that R_{in} can be affected. Larger cells have lower R_{in} values due to the increased membrane surface area times the specific membrane resistivity, such as adult versus neonatal cardiac myocytes. Alternatively, a lower R_s value in parallel with R_m will reduce R_{in} by the relative proportion of $R_m/(R_s + R_m)$. Alterations in R_{in} are the most likely experimental variable during dual whole-cell recordings using the same cell preparation. To model the effect of a reduced R_{in} on I_j and R_j estimates, R_{s1} and R_{s2} were lowered to 1 GΩ each. Because R_{m1} and R_{m2} also equal 1 GΩ, R_{in1} and R_{in2} drop to 0.50 GΩ. The effects are threefold. I_{in} will approximately double for the same command potential V, the series resistance factor will be approximately doubled, and any intrinsic E_{rest} will be further shunted, causing an additional increase in I_{in}. Given that R_{in} is still a relatively high 500 MΩ, I_{in} will increase by only 2 pA/mV difference in $V - E_{rest}$. For $V_1 = V_2$ at -40 mV, this results in an increase in I_{in} from -3.5 to -40 pA, or only an additional 400 μV initial voltage drop across each electrode. These modest alterations in the dual whole-cell circuit increases the percent error in the R_j estimates using Eqs. 5a and 5b only slightly to -2.5% compared to $+43\%$ for Eq. 5c. However, large errors in the estimation of I_j and R_j occur if E_{rest2} is considered to be 0 mV as in Eq. 1f (Eq. A9 in Van Rijen et al., 1998). These large errors in the estimation of I_j cause the R_j estimate to fluctuate from large negative to large positive values of percent error eventually stabilizing within ±2% error when $R_j \leq 100$ MΩ (data not shown, see Fig. 3).

Holding and resting potential discrepancies. Errors in the estimation of I_j and I_{in} from whole-cell currents can also arise from differences in the common holding potential of the dual-cell voltage clamp and the intrinsic resting potential of a myocyte or neuron. To model an E_{rest} of -80 mV, I_{rest} was increased to -80 pA. In the whole-cell configuration with $R_s = 10$ GΩ, E_{rest} decreased to -72.7 mV. Maintaining a $V_1 = V_2$ value of -40 mV again imposes an I_{in} value that will often exceed the value of I_j and produce significant errors in the R_j estimate unless E_{rest} is appropriately considered as in Eq. 5a. Given the optimal R_{el}/R_{in} of 1.1% and $R_{in} \approx 1$ GΩ, the effects of the additional $+36$ pA of I_{in} are negligible and the R_j estimates with Eqs. 5a and 5b remain within -1.5% error as the uncompensated R_j estimate rises to $+42\%$ at $R_j = 50$ MΩ.

Whatever the cause of an increase in I_{in}, ΔV_m will increase and accurate estimates of I_{in} become more critical when I_j is low if Eq. 5a is to be used to estimate R_j. Baseline subtraction of all whole-cell currents when $V_1 = V_2$ offers the advantage of being insensitive to the initial value of I_{in} and any changes in I_{in} during a dual whole-cell recording can be accurately monitored by tracking the baseline value of I_2 during an experiment. Another feature of Eq. 5b that is not apparent from the average percent error values illustrated in Fig. 2 *A* is the behavior as a function of V_j. To illustrate the differences between Eqs. 5a and 5b under more realistic dual whole-cell conditions, slight asymmetries were assigned to the circuit and the R_j estimates over a ±100 mV were evaluated.

Realistic experimental conditions

On average, the 4–5 MΩ patch electrode acquires an R_{el} of 20 MΩ after patch break (Wang et al., 1992), $R_j \cong 200$–500 MΩ (Veenstra et al., 1992; Beblo et al., 1995), and the R_{in} of connexin-transfected N2A cells ≥1 GΩ. Small asymmetries were assigned to R_{el} and R_{in} to mimic realistic experimental conditions as listed in Table 1. The common holding potential of -40 mV also differs slightly from E_{rest} because the value of E_{rest} is typically not evaluated before beginning an experiment. The results are illustrated in Fig. 3 where Eqs. 5a and 5b again provide similar R_j estimates of 490 MΩ, or -2.0% error. The uncompensated R_j estimate was 555 MΩ or $+11.1\%$ error. Eqs. 1g and 1i also produced similar I_j estimates that differed by a maximum of 1.0 pA with an average percent error from ideal I_j values of -8.3%. What was not readily apparent from Fig. 3 *B* was that the standard deviation of the percent error in I_j was 0.5% with Eq. 1i and $<0.2 \times 10^{-6}\%$ with Eq. 1g. This again illustrates the better stability of Eqs. 1g and 5b in estimating I_j and R_j. If E_{rest2} is omitted from the I_j estimation (Eq. 1f), I_j is shifted by $+20$ pA and the percent error rises sharply at low V_j values where I_j is small (Fig. 3 *A*). This results in R_j estimates that also fluctuate toward negative and positive extremes as I_j approaches 0 pA (Fig. 3 *A*). This is similar to the variations in R_j obtained when E_{rest2} is omitted from the I_j estimates for the low R_{in} and high E_{rest2} examples. The asymmetry in the actual V_j was only 200 μV and the percent error was 10.1% (Fig. 3 *C*). Eq. 5b produces stable R_j estimates, provided that R_{in2} remains stable, whereas Eq. 5a is very sensitive to the I_{in2} estimate at each V_j analyzed. The accuracy of both correction methods is comparable when performed correctly to within 5% error for $R_j \leq 50$ MΩ although Eq. 5b has the advantages of requiring a simpler calculation of I_j and better stability over a range of V_j values.

In Figs. 2 and 3, the compensated R_j estimates of Eqs. 5a and 5b underestimated R_j by 1 to 4%, depending on the dual

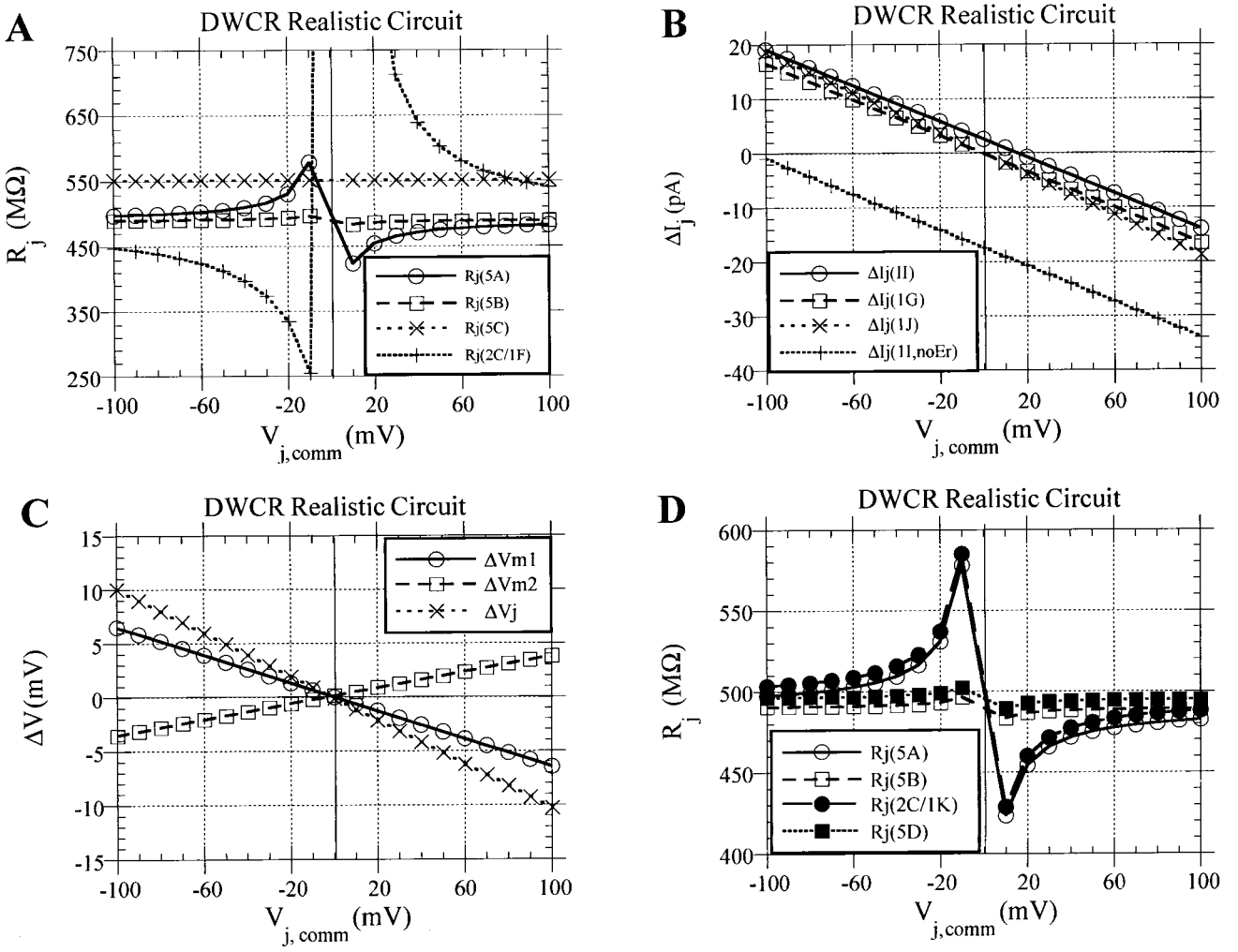

FIGURE 3 R_j, I_j, and V_j measurements under realistic dual whole-cell conditions. (*A*) R_j estimates obtained by Eqs. 5a, 5b, 5c, and 2c/1f for a fixed R_j = 500 MΩ with modest asymmetries in the R_{el} and R_{in} values (see Table 1 for details). Compensated R_j estimates (Eq. 5a and 5b) were within 2% error, whereas the uncompensated R_j estimate (Eq. 5c) overestimated R_j by 11%. Omitting the E_{rest2} term from the I_{in2} calculation (Eq. 1f) produced less stable R_j estimates when I_j is small relative to I_{in2} that approach the compensated R_j estimates at higher V_j values. (*B*) I_j estimates obtained using the compensated $-\Delta I_2$ (Eq. 1g), Kirchoff's law equation for I_2 (Eq. 1i), Kirchoff's law equation for I_2 with the E_{rest2} term omitted (Eq. 1f), or uncompensated $-\Delta I_2$ (Eq. 1j) methods. The compensated I_j estimates differed by less than 1 pA except when the E_{rest2} term (= −33.3 mV) was omitted from the I_{in2} calculation. The resulting 20-pA shift in the I_j–V_j relationship produces larger variations in the R_j estimate as V_j approaches 0 mV. Because R_{el}/R_{in} were 1.9% and 1.2% for cells 1 and 2, the uncompensated I_j estimate varied by only an additional 1.2% from the compensated I_j values. (*C*) The deviation in V_{m1}, V_{m2}, and total V_j (Eq. 2a–c) from the applied command potentials, V, for the dual whole-cell conditions described in parts *A* and *B*. The total decrease in V_j closely paralleled the ≅10% reduction in the uncompensated I_j estimate relative to the ideal circuit. Both Eqs. 1g and 1i increased the I_j estimate by 1.2% due to the value of R_{el2}/R_{in2}. (*D*) The same R_j estimates from panel *A* before and after omitting the $[1 + (R_{el2}/R_{in2})]$ compensation factor from Eq. 5a (Eq. 2c/1k) and Eq. 5b (Eq. 5d). Because the $-I_2 \cdot (R_{el2}/R_{in2})$ term is equivalent to the fraction of I_j that flows across R_{in2} to produce ΔV_{m2}, the correction for ΔV_{m2} cannot occur in both the corrected V_j and I_j terms of the R_j estimate.

whole-cell recording conditions. Figure 3 *B* illustrates the point that the recorded $-\Delta I_2$ current (Eq. 1j) closely matched the drop in V_j across the dual patch clamp circuit (Eq. 2c), whereas Eqs. 1g and 1i compensated for the fraction of I_j that flowed across R_{in2} instead of R_{el2}. However, it follows that the alteration in V_2 produced by $\Delta I_2 \cdot R_{el2}$ must equal $\Delta I_{in2} \cdot R_{in2}$ because, by definition, both must equal ΔV_{m2} (see Eq. 2d). This means that the previously published Eqs. 2c/1f and 5b for corrected R_j estimates contain a small error (Veenstra and Brink, 1992; Van Rijen et al., 1998). If Eq. 2c is to be used to calculate the actual applied V_j, then the whole-cell current attenuation factor $[1 + (R_{el}/R_{in})]$ must not reappear in the denominator of Eqs. 5a and 5b. To test this derivation, Eq. 1i was modified to

$$I_j = -I_2 + \frac{(V_2 - E_{rest2})}{R_{in2}} \qquad (1k)$$

and Eqs. 2c/1j to

$$R_j = \frac{[(V_1 + \Delta V_1) - V_2] - [(R_{el1} \cdot I_1) - (R_{el2} \cdot I_2)] - E_{rev}}{-\Delta I_2}. \quad (5d)$$

The results are shown in Fig. 3 *D* where the percent error in the compensated R_j estimates for the realistic dual whole-cell circuit is illustrated. The percent error was reduced from −1.1, −2.3, and −2.0% to −0.04, −0.18, and −1.25% for the $R_{el} = 10$ MΩ, 20 MΩ, and realistic circuits when Eq. 5d was used to estimate R_j (= 500 MΩ) instead of Eq. 5b. The difference in the percent error between Eq. 5a and 2c/1k or Eq. 5c and 5d, equal to R_{el}/R_{in}, was typically <2% for all dual whole-cell conditions examined. Eq. 5d was most accurate (<0.5%) when symmetry was maintained for the dual whole-cell circuit. Even though Eqs. 5a and 5b remain accurate to within −5% over a 100-fold range of R_j values, Eq. 5d remains more accurate than Eq. 5b by the percentage equivalent of R_{el2}/R_{in2} under actual dual whole-cell experimental conditions where R_j is unknown.

Alternative recording configurations

The limitations and possible errors of estimating I_j and R_j in the dual whole-cell configuration are evident from Eqs. 5a and 5b. An alternative method for studying the regulation of R_j was developed using adult cardiac myocytes (Noma and Tsuboi, 1987; Sugiura et al., 1990). The "open-cell" configuration relies on R_{in1} measurements obtained after R_{in2} was shunted to 0 Ω. This configuration was modeled using the circuit diagram in Fig. 1 by setting R_{el2} and $R_{in2} = 0$ Ω. Because $V_2 = 0$ mV, the common holding potential for minimizing I_j becomes $V_1 = 0$ mV. Another worthy consideration of these initial open-cell conditions is the effect on E_{rest1} now that R_j and R_{in1} are in parallel. The net resistance of the open-cell (R_{oc}) is

$$R_{oc} = \frac{R_{in1} \cdot R_j}{R_{in1} + R_j}, \quad (9)$$

the open-cell current (I_{oc}) when $V_1 = 0$ mV is

$$I_{oc} = I_{rest1} + \frac{E_{rev}}{R_j}, \quad (10)$$

and the open cell voltage (E_{oc}) is

$$E_{oc} = \left[I_{rest1} + \left(\frac{E_{rev}}{R_j} \right) \right] \cdot R_{oc}. \quad (11)$$

It is apparent that it is advantageous to obtain the values of R_{in1}, R_j, and E_{rest1} prior to formation of the open-cell configuration to improve the accuracy of the subsequent R_j estimates. Furthermore, these circuit analyses are best performed with the same intracellular pipette solution in the external bath because this will create symmetrical ionic conditions upon the initial formation of the open-cell configuration (i.e., $E_{rev} = 0$ mV). Because R_{in1} is in parallel with R_j, any experimental variable designed to alter R_j must not affect R_{in1} since these two values cannot be independently determined. Control single whole-cell experiments are required to assess the action of any test solution on R_m (R_{in}) of the cell preparation. In the open-cell configuration when $V_1 \neq 0$ mV, I_1 is

$$I_1 = \frac{V_1}{R_{el1} + R_{oc}} - \left(\frac{E_{oc}}{R_{oc}} \right) = \frac{V_1 \cdot R_{oc} - E_{oc} \cdot (R_{el1} + R_{oc})}{(R_{el1} + R_{oc}) \cdot R_{oc}} \quad (4e)$$

or

$$I_1 = \frac{V_1 \cdot R_{in1} - E_{rest1} \cdot (R_{el1} + R_{in1})}{(R_{el1} + R_{in1}) \cdot R_{in1}} + \left[\frac{[(V_1) \cdot R_j] - [E_{rev} \cdot (R_{el1} + R_j)]}{(R_{el1} + R_j) \cdot R_j} \right]. \quad (4c)$$

This equation applies to any whole-cell macroscopic current in the open-cell configuration. The open-cell preparation can result from a coupled cell pair, a freshly isolated cell containing functional gap junctions, or a single cell with functional connexin hemichannels (Mazet et al., 1985; Noma and Tsuboi, 1987; Sugiura et al., 1990; Zhou et al., 1997; Zhang et al., 1998). These conditions do not apply to direct patch recordings of hemichannels or gap junction channels in the cell-attached patch or excised patch configurations originally described during the development of the patch clamp technique (Hamill et al., 1981; Sakmann and Neher, 1995).

Open-cell R_j measurements

The whole-cell currents were modeled using Eq. 4c for a range of R_j and R_{in1} values. The *I–V* curves obtained in the open-cell configuration with $R_j = \infty$, 1.0 GΩ, or 0.5 GΩ are illustrated in Fig. 4 *A*. R_{oc} was estimated from 1/slope of the linear *I–V* plot and the actual and measured values are listed in Table 2. The corresponding R_j value was calculated using Eq. 9.

Because R_{el}/R_{oc} was only 1.1%, the *I–V* plots overestimated R_{oc} by 1–4.3%, whereas the $I–V_m$ plots were accurate to within −1.5% at all values tested. The R_{el}/R_{oc} ratio increased to 2.0% for $R_s = 1$ GΩ and decreased to 0.8% for $R_m = 1.5$ GΩ. The R_j estimates in Table 2 account for the changes in R_j, R_s, and R_m of the model circuit. However, in an open-cell experiment, where the change in R_{in} was not accounted for, the R_j estimates would be 354.4 and 616.6 MΩ, respectively. Using the slope of the $I–V_m$ plot does not improve these estimates (335.4 and 589.9 MΩ) because the ≈30 and 20% errors are due to the estimate of R_{in}. The only

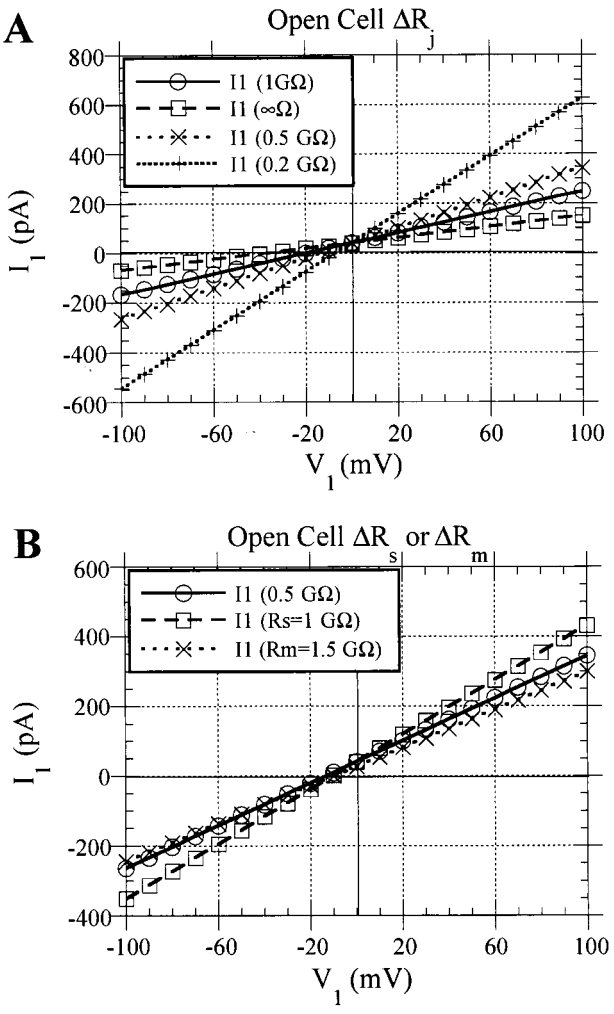

FIGURE 4 Whole cell *I–V* relationships in the open cell configuration ($R_{el2} = R_{s2} = R_{m2} = 0\ \Omega$). (*A*) The slope conductance = $1/R_{oc}$, so calculation of R_j requires exact knowledge of R_{in1} prior to shunting cell 2. Subtraction of the *I–V*s when R_j is finite (1.0, 0.5, or 0.2 GΩ) by $R_j = \infty$ ($R_{oc} = R_{in1}$) provides an accurate measure of R_j, provided that V_{m1} is calculated from V_1 using Eq. 2a. All other cell parameters were optimal (see Table 2). (*B*) The effect of changes in R_{in1} on the open cell *I–V* relationship with a constant R_j. A 50% increase in R_m models a nonspecific membrane conductance decrease due to K^+ substitution by Na^+. A reduction in R_s from 10 to 1 GΩ reduced R_{in1} by 45%. The effects of changes in R_{in1} on R_{oc} are summarized in Table 2.

possible way to account for a change in R_s is to return to a control condition where R_{oc} was known initially, otherwise changes in R_s will dramatically affect the R_j estimate in the open-cell configuration.

Experimental application of I_j and R_j correction methods

Assessment of cellular and junctional parameters

To assess the feasibility of these two correction methods relative to an uncompensated R_j estimate, Eqs. 5a–c were applied to dual whole-cell current recordings from rCx40-transfected N2A cells. R_{el} was determined from Eq. 6 in response to a 10-ms, −40 to −35-mV voltage step applied simultaneously to both cells. To obtain all of the necessary cellular parameters, both cells were simultaneously ramped from −140 to +60 mV from a common holding potential of −40 mV. The whole-cell current traces from one experiment are illustrated in Fig. 5. The R_{in1} and R_{in2} values were 3.6 and 1.5 GΩ as determined from trace 1 in the −140 to −20-mV range. The command potential (V_{comm}) was varied by 1 mV per 20 ms. The slope of the *I–V* curve was determined for each cell by linear regression analysis over the linear range of the *I–V* curve and E_{rest} was determined for each cell by solving for the condition of $I_1 + I_2 = 0$ to obtain the value of V_{comm} necessary for Eq. 8b. Alternatively, the value of E_{rest} can be determined directly from the common value of V_m where $I_1 + I_2 = 0$ in the two $I–V_m$ plots. V_m was calculated from the whole-cell currents using Eqs. 2a and 2b. The value of g_j was subsequently determined from the same voltage ramp applied alternately to cell 1 and cell 2 (Fig. 5, *traces 2 and 3*) to generate the corresponding $I_j–V_j$ plots. The R_j measurements of 169 and 200 MΩ from traces 2 and 3 with Eqs. 5a, 5b, or 2c/1f were calculated from the reciprocal of the linear slope in the −20 to +20-mV range. Eqs. 2c/1k and 5d produced identical slopes with slightly higher R_j values (173 and 202 MΩ, Fig. 6, *A* and *B*). The respective uncompensated R_j measurements were 232 and 262 MΩ. These ≥30% higher R_j measurements occurred even though the R_{el}/R_{in} ratios were only 0.75% and 1.95% for cells 1 and 2 because the $(R_{el1} + R_{el2})/R_j$ ratio was ≥29%. The significance of including E_{rest} in the Kirchoff's law solution to I_j was also examined by omitting this term from Eq. 5a (Fig. 6, *A* and *B*, data not shown).

The results of four rCx40 cell pairs revealed only two differences between the four R_j estimates. Eq. 5c, the uncompensated R_j estimate, overestimated R_j in every experiment, whereas Eqs. 2c/1k and 5d always produced identical slopes of the $I_j–V_j$ curves. The effect of omitting the E_{rest} term from the I_j estimate was a parallel shift in the $I_j–V_j$ curve along the V_j axis. The *x*-intercept was ≤1 mV in three of four experiments using Eqs. 5c and 5d. The value of the *x*-intercept was higher in three of four experiments using Eq. 2c/1k and exceeded 1 mV in 50% of the $I_j–V_j$ curves. Omitting the E_{rest} term from Eq. 1k produced higher voltage offsets in 50% of the cases.

One advantage of this approach is that an estimate of R_j can be obtained in both directions from the slope of the linear region of the $I_j–V_j$ plots. Asymmetries in the dual whole-cell circuit can be accurately assessed from the data acquired in <1 min. Another advantage is that g_j (or R_j) can be calculated in a continuous manner over a ±100-mV range. The primary disadvantage is that I_j is obtained in an asymmetric manner relative to $+V_j$ and $-V_j$ values because each V_j ramp commenced with a large V_j value and ap-

TABLE 2 Open cell measurements of R_j from *I–V* plots

Resistance Value (GΩ)	Actual R_{oc}* (MΩ)	R_{in1} (MΩ)	1/slope *I–V* (MΩ)	R_j† (MΩ)	1/slope $I–V_m$‡ (MΩ)	R_j† (MΩ)
$R_j = \infty$ (10^{+9})	909.1	909.1	918.9	85.2 GΩ	908.8	2.75 TΩ
$R_j = 1$	476.2	909.1	481.1	1022	471.1	977.8
$R_j = 0.5$	322.6	909.1	327.9	512.9	318.0	489.1
$R_j = 0.2$	163.9	909.1	170.9	210.5	160.9	195.5
$R_s = 1$§	250.0	500	255.0	520.4	245.0	480.4
$R_m = 1.5$§	361.5	1300	367.4	512.1	357.4	492.3

*Actual R_{oc} was calculated using Eq. 9 with R_s = 10 GΩ, R_m = 1.0 GΩ, and R_{el} = 10 MΩ unless otherwise indicated.
†R_j was calculated from Eq. 9.
‡V_{m1} was calculated with Eq. 2a and the $I_1–V_{m1}$ plot was fitted by linear regression.
§R_j = 0.5 GΩ for all calculations.

proached the opposite V_j polarity from an initial value of 0 mV. This is best illustrated in Fig. 6, where the $I_j–V_j$ and $g_j–V_j$ plots for the experiment shown in Fig. 5 are presented. When V_j is calculated using Eq. 2c, the large transient in I_j in response to an instantaneous −100-mV V_{comm} step occurs on opposite ends of the $I_j–V_j$ curve (Fig. 6, *A* and *B*). The apparent asymmetry in the applied V_j prevents valid comparisons of V_j-dependent changes in g_j at opposite V_j values. The I_j transient also illustrates the point that V_j is changing during the initial voltage step because the value of $I \cdot R_{el}$ is changing in time. This could explain the variability observed in the decay time constants of I_j in previous reports of V_j-dependent gating (Veenstra, 1991b; Wilders and Jongsma, 1992; Wang et al., 1992; Chanson et al., 1993).

The $g_j–V_j$ curves calculated with Eqs. 5d or 2c/1k also illustrate the differences in the $-\Delta I_2$ (Eq. 1g) and $-I_2 + I_{in2}$ (Eq. 1k) approaches to estimating I_j. Anytime I_j or V_j approaches 0, the R_j and g_j estimates become unstable and approach $\pm\infty$. These fluctuations in the g_j estimates are generally larger with Eq. 2c/1k than with Eq. 5d. The g_j fluctuations were closer to 0 mV with Eq. 5d because the *x*-intercept is also smaller relative to Eq. 2c/1k (Fig. 6, *C* and *D*).

V_j-dependent regulation of g_j

Because the steady-state $G_j–V_j$ curve for rCx40 derived from a conventional voltage pulse protocol was already known (Beblo et al., 1995), we chose to reexamine the intrinsic V_j-gating of rCx40. The primary disadvantage of the V_j ramp was alleviated by gradually increasing V_j from 0 mV in both directions and the ramp speed was varied to determine what ramp duration was required to continuously approximate steady-state g_j values. V_1 was varied from −40 to −140 mV and from −40 to +60 mV in 1-mV increments with rest intervals of varying duration between each voltage ramp to allow for recovery from any V_j-gating that might have occurred. Each V_1 ramp was repeated five times and the I_1 and I_2 traces were ensemble averaged prior to calculation of I_j, V_j, and g_j. Ramp durations of 5, 10, 15, 20, 25, 30, 40, 50, 100, and 200 ms/mV were repeated five times on each of five cell pairs. The results from one experiment are shown in Fig. 7 *A* that demonstrate the progression toward steady-state values with increasing ramp duration. Only Eq. 1j was used to estimate I_j because Eq. 5d produced accurate and more stable R_j estimates than did Eq. 2c/1k without requiring determination of E_{rest2} values. All continuous $I_j–V_j$ relationships were linear in the V_j range of ±25 mV. The slope of the $I_j–V_j$ relationship in the 0 to ±25-mV V_j range was used to normalize g_j (G_j) of each experiment. The $G_j–V_j$ curve was fitted by the equation

$$G_j = \frac{G_{max} - G_{min}}{1 + \exp[(zF/RT)(V_j - V_{1/2})]}, \qquad (12)$$

with pClamp8.0 software (Axon Instruments, Inc., Foster City, CA).

The G_{max} and G_{min} values were constant for all voltage ramp speeds (5, 10, 15, 20, 25, 30, 40, 50, 100, and 200 ms/mV). The average $G_{max} = 1.01 \pm 0.01$ and the average $G_{min} = 0.24 \pm 0.04$ for all ten voltage ramp durations. The half-inactivation voltage ($V_{1/2}$) and gating charge valence (z) values varied reciprocally with the voltage ramp speed as illustrated in Fig. 7, *B* and *C*. The $V_{1/2}$ and z values for $-V_j$ and $+V_j$ were fitted with a single exponential function to determine the time constant (τ) for each process. The standard deviations were $V_{1/2} < 0.8$ mV and $z < 0.10$ for each data point. The $\tau_{V_{1/2}}$ was 36 ± 8 and 23 ± 6 ms/mV for $-V_j$ and $+V_j$ and τ_z was 81 and 149 ms/mV. Because V_j was not constant, τ possesses the units of ms/mV. The time-dependence of these G_j-gating parameters has not been previously described. The shortest ramp duration of 5 ms/mV ensured that the voltage clamp had achieved steady state prior to the next 1 mV step for all experiments. Figure 7 *C* indicates that, as soon as V_j was stable, a net valence of approximately two gating charges had already moved (i.e., instantaneous) with another 1.5–2.0 charges to follow with a τ of approximately 80–150 ms. This suggests that part of the rCx40 V_j-gate is located within the V_j field while another

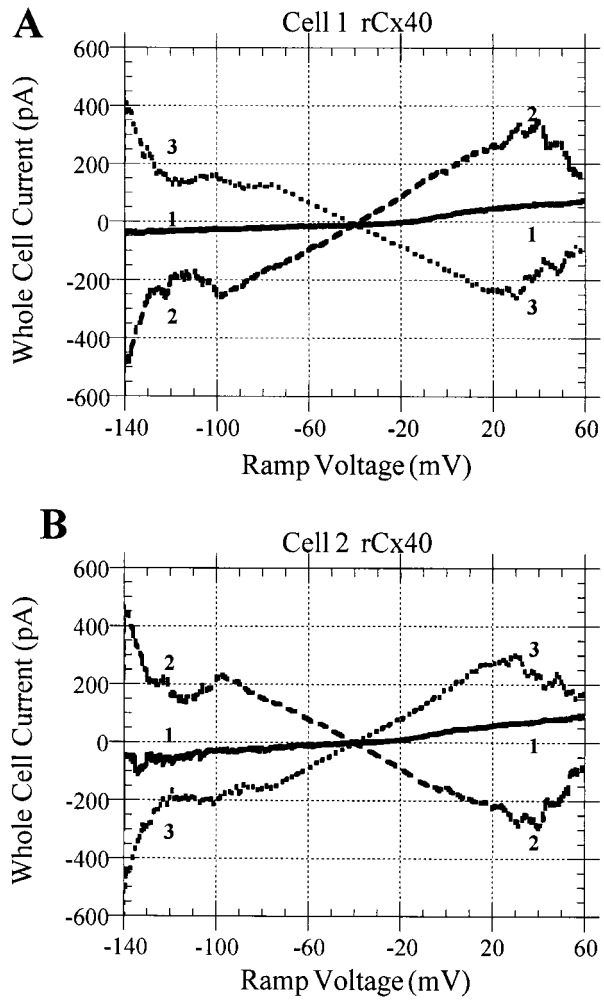

FIGURE 5 Experimental determination of R_{in}. A voltage ramp from −140 to +60 with a slope of 0.05 V/s (i.e., 20-mS/mV increment) was applied sequentially to both cells simultaneously (*trace 1*), cell 1 alone (*trace 2*), and cell 2 alone (*trace 3*) from a common holding potential of −40 mV. The corresponding whole-cell current traces are shown for (*A*) cell 1 and (*B*) cell 2. R_{in} was calculated from the slope of trace 1 after calculating V_m for each cell. Only $V_m < -20$ mV was used to calculate R_{in} for N2A cells. R_{el1} and R_{el2}, previously determined from whole-cell capacitive transient decay constants, were 28 and 30 MΩ. R_{in1} and R_{in2} were 3.6 and 1.5 GΩ, and the resulting series resistance errors were 0.8% and 2.0%, respectively. E_{rest} was −24.5 ± 0.2 mV for both cells. I_j was calculated from traces 2 in panel *B* and 3 in panel *A* for the purpose of estimating R_j.

component of approximately equal charge moves into the V_j field with a finite reaction rate that can be determined using a variable duration voltage ramp method. The final values for $V_{1/2}$ and z also closely approximate the previously determined values for rCx40 using a conventional voltage step protocol.

Because the $V_{1/2}$ converged to a constant value for the 100 and 200-ms/mV duration V_j ramps, the 200-ms/mV G_j–V_j curves were compared to the steady-state G_j curve for rCx40 obtained using a 6-s duration pulse protocol (Beblo et al., 1995). The results from six rCx40 cell pairs are summarized in Fig. 8 *A* and Table 3. The slope of the instantaneous I_j–V_j relationship was used to normalize g_j for each experiment from Beblo et al. (1995). Because there was no instantaneous I_j–V_j relationship for the ramp protocols, the linear slope of the 0 to ±25-mV I_j–V_j relationships were used to normalize the g_j of each experiment. The mean g_j was 2.74 ± 2.58 and 2.49 ± 2.05 nS for the six $-V_j$ and $+V_j$ ramps compared to 2.26 ± 1.50 nS from previous results ($N = 28$, only 10 were used for the Boltzmann fit, Beblo et al., 1995). The slight reduction in the mean slope g_j between $-V_j$ and $+V_j$ ramps indicates that the 15-s rest interval needs to be extended to permit full recovery from V_j-dependent inactivation.

A pulse protocol similar to the one used in Beblo et al. (1995) was also applied to the same six rCx40 cell pairs (Fig. 8 *B*). The mean g_j was 2.79 ± 2.11 nS for the six instantaneous I_j–V_j relationships ($r \geq 0.97$ except for the lowest g_j experiment, $r = 0.93$). The best fit with Eq. 12 to this data set yielded $G_{max} = 1.13 \pm 0.23$ or 0.81 ± 0.06, $G_{min} = 0.20 \pm 0.07$ or 0.23 ± 0.05, $V_{1/2} = -34.9 \pm 8.2$ or $+44.2 \pm 3.8$, and $z = -1.7 \pm 0.7$ or $+4.0 \pm 2.1$ for $-V_j$ and $+V_j$ values. The mean instantaneous and steady state g_j values were 2.81 ± 2.17 and 2.45 ± 2.06 nS. These results further demonstrate the advantage of the continuous V_j ramp over the pulse protocol in producing steady state G_j–V_j results with reduced variability from the same experimental population. Each ensemble-averaged V_j ramp was acquired in the same amount of time as a single V_j pulse protocol.

DISCUSSION

The most sensitive assay for gap junction communication is electrical current because it can be resolved to the level of a single channel. The regulation of gap junction communication typically requires only the assessment of the value of R_j or g_j in response to the modulating treatment. There are limitations to the measurement of R_j from dual whole-cell patch clamp recordings that are often not appreciated. Two related methods of correcting for series resistance errors in the estimation of I_j, V_j, and R_j have been published (Veenstra and Brink, 1992; Van Rijen et al., 1998). Neither of these methods considered the possible effects of physiological cellular resting potentials or gap junction diffusion potentials on these electrical measurements. The derivations presented in this manuscript provide the mathematical solutions to these "real" cell conditions and assess the performance of the Kirchoff's law (Eqs. 1h and 1i) and baseline subtraction expressions (Eqs. 1g and 1j) for I_j under a variety of experimental conditions that mimic actual dual whole-cell experimental conditions. The experimental determination of nonzero E_{rev} values will be considered in another manuscript on relative ionic permeability measurements of gap junction channels.

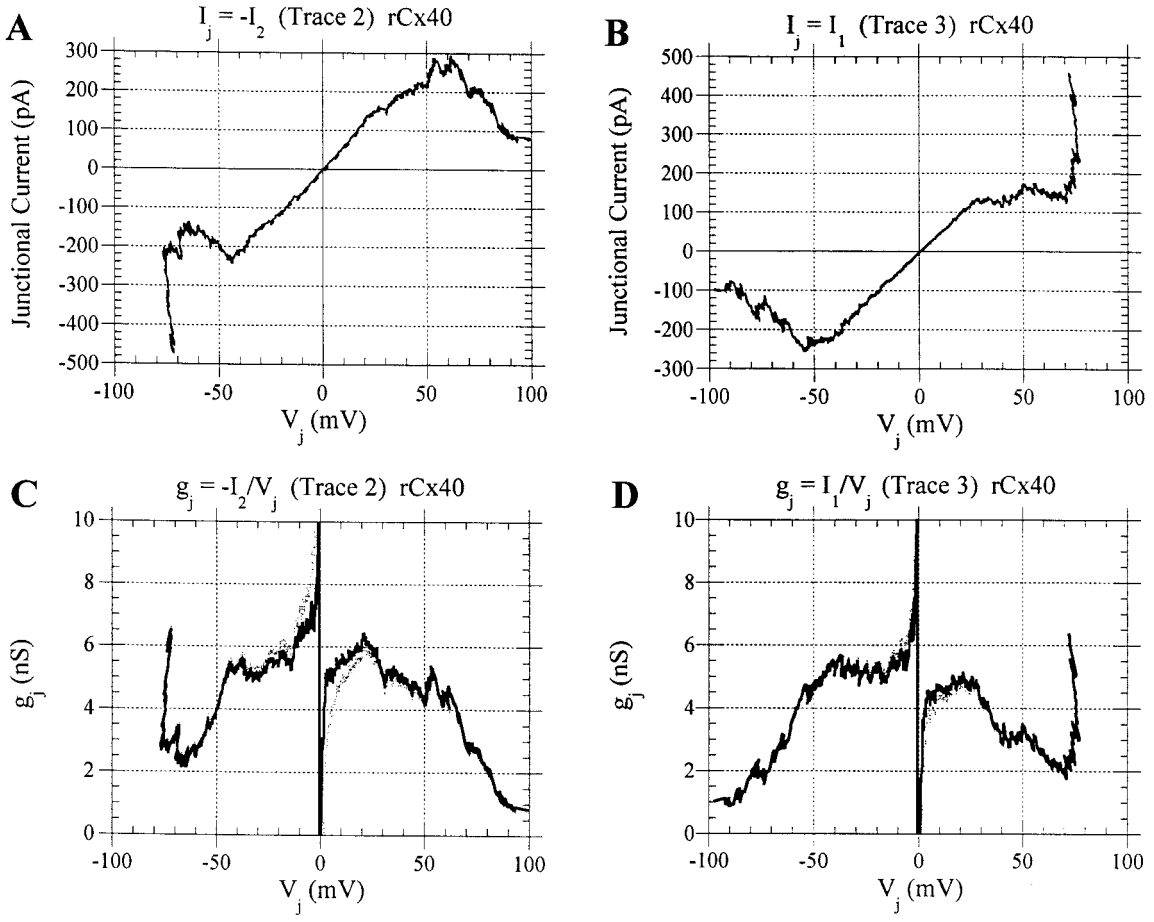

FIGURE 6 Experimental R_j measurements. (*A*) I_j–V_j relationship derived from trace 2 in panel *B* of Fig. 5 according to Eq. 1j (*solid line*) and 1k (*dashed line*). The linear slope between −20 and +20 mV was 5.78 nS (R_j = 173 MΩ). The voltage offsets were +0.5 and +4.3 mV, respectively (+10.5 mV for Eq. 1k with the E_{rest2} term omitted). (*B*) I_j–V_j relationship derived from trace 3 in panel *A* of Fig. 5 according to Eq. 1j (*solid line*, ΔI_1 replaces $-\Delta I_2$) and Eq. 1h (*dashed line*, less the current compensation factor). The linear slope between −20 and +20 mV was 4.95 nS (R_j = 202 MΩ). The voltage offsets were +0.9 and +1.4 mV, respectively (+0.1 mV for Eq. 1e less the current compensation factor). (*C*) g_j–V_j curves for the I_j traces shown in part *A*. The fluctuations in the continuous g_j calculations are greater for Eq. 2c/1k (*dotted line*) than the $-\Delta I_2$ method (Eq. 5d, *solid line*). Both methods produce similar g_j values at higher V_j. The effect of an instantaneous −100-mV command step in V_j is apparent at the left margin of both traces. (*D*) g_j–V_j curves for the I_j traces shown in part *B*. Ramping cell 2 instead of cell 1 produces a more stable continuous g_j curve, perhaps because cell 1 had the higher R_{in} and lower R_{el}/R_{in} ratio of the cell pair. The results with Eq. 2c/1h (less the current compensation factor, *dotted line*) are indistinguishable from the ΔI_1 method (*solid line*).

The results presented in Figs. 2 and 3 demonstrate that both methods are accurate to within 5% error even with 20-nS g_j cell pairs and 50 MΩ whole-cell patch electrodes. The differences in the two correction methods are most prevalent when I_j is small and variations in the estimate of I_{in} from the whole-cell current dramatically influence the relative value of I_j. Because Eq. 1g results from the baseline subtraction of Eq. 1i when $V_1 = V + \Delta V$ and $V = V_1 = V_2$, the only expected difference between these two expressions will result from different assessments as to the value of $I_{in2} = V_2/R_{in2}$ (Eq. 1f; Eq. A9 in Van Rijen et al., 1998). The effect of this one difference is illustrated in Figs. 5 and 6 where the variations in the g_j estimate increase as V_j, and necessarily I_j, nears zero. The model and experimental results of dual whole-cell recordings demonstrate that the $-\Delta I_2$ expression is inherently more stable than the $-I_2 + I_{in2}$ expressions derived from Kirchoff's law. As expected from the initial conditions, the stability of the $-\Delta I_2$ method depends on the stability of the I_2 ($V_1 = V_2$) baseline, not the value of V_2/R_{in2} as is true for the Kirchoff's law I_j equation. This is true even when the value of E_{rest2} is included in the I_{in2} calculation (Eq. 1i). Eq. 1g also outperformed Eqs. 1f and 1i in 75% of the experiments in estimating the *x*-intercept of the I_j–V_j relationship to be nearest to 0 mV (<1 mV error). Because it is not necessary to calculate E_{rest} to estimate I_j when using the ΔI approach, this method is also easier to implement experimentally. Except when I_j is small, the two approaches agree very closely. So either method is acceptable although the ease of use and stability of the I_j measurements favor the use of the $-\Delta I_2$ method. Another

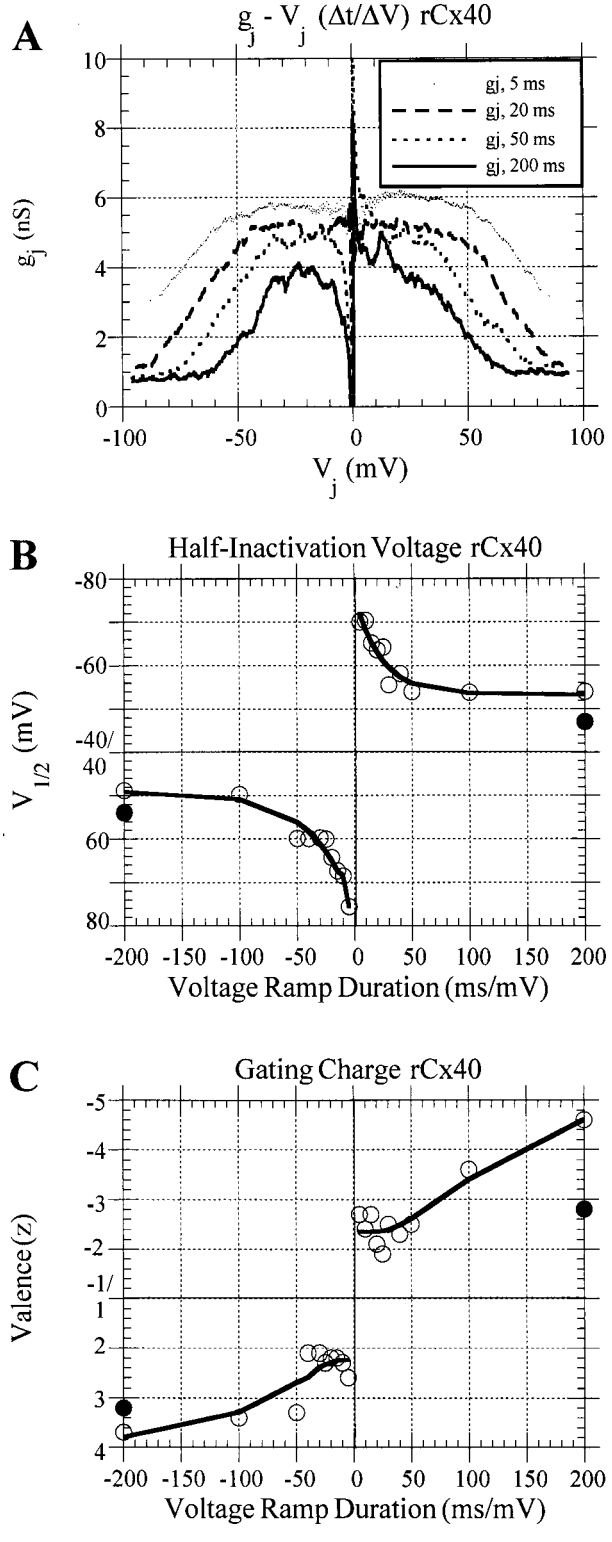

FIGURE 7 The time-dependence of $V_{1/2}$ and z. (*A*) Four g_j–V_j curves from one rCx40 experiment illustrate the time-dependent changes in g_j that occur with different ramp durations (5, 20, 50, and 200 ms/mV). The $-25 \geq V_j \geq 0$ and $0 \leq V_j \leq +25$ mV linear g_j values were 5.6 and 5.8, 5.1 and 5.2, 4.6 and 5.4, and 3.4 and 4.3 nS for the 5, 20, 50, and 200 ms/mV ramps, respectively. (*B*) The ensemble-averaged G_j–V_j curves from 5–6 rCx40 experiments were fitted with Eq. 12 and the value of the half-inactivation voltage, $V_{1/2}$, for 10 different V_j ramps were fitted with a single exponential function to determine the time constant. The solid points represent the value of $V_{1/2}$ obtained from a conventional long-pulse voltage protocol (Beblo et al., 1995). The $V_{1/2}$ converged toward a final value of -49 or $+53$ mV with a time constant of 36 or 23 ms/mV. $G_{max} = 1.03$ and $G_{min} = 0.23$ were constant for all slope voltages. $N = 5$ for all ramp durations except the 200-ms/mV ramp ($N = 6$). (*C*) The net valence (z) of the gating charge movements for the same data shown in panel *B*. The solid points again represent the value of z obtained from a conventional long-pulse voltage protocol (Beblo et al., 1995). The initial value of z was ± 2.3 ($\pm V_j$) and it converged to final values of -3.8 and $+4.6$ with time constants of 81 and 149 ms/mV.

advantage is that on-line monitoring of the value of I_2 when $V_1 = V_2$ throughout the experiment is easy to perform and provides a necessary check of the condition that I_{in2} remain stable for the duration of the dual whole-cell experiment (Veenstra and Brink, 1992). Both Eqs. 1g and 1i take into account the current divider circuit formed by R_{el} and R_{in} of the (postjunctional) cell selected to record I_j. This is important if V_2 is to be used in the R_j calculations. However, the voltage difference $V_{m1} - V_{m2}$ (Eq. 2c) is measured between the nodes located central to R_{el} and R_{in}. Therefore, if Eq. 2c is used to calculate V_j, then the whole-cell current attenuation factor $[1 + (R_{el}/R_{in})]$ produced by the current divider circuit must not be included in the I_j calculations (substitute Eq. 1j for 1g and 1k for 1i). Eq. 2c/1k should be substituted for Eq. 5a and Eq. 5d for Eq. 5b in all and subsequent R_j calculations. Alternatively, one must use V_2 and the current attenuation factor to calculate V_j and I_j to avoid double compensation of ΔV_{m2}. The important point is that one must use the same two nodes to record junctional voltage and current (i.e., V_1 and V_2 or V_{m1} and V_{m2}). Previously published correction methods for dual whole-cell junctional current and voltage measurements incorrectly overcompensated for the series resistance errors due to R_{el2} in both the junctional current and voltage equations (Veenstra and Brink, 1992; Van Rijen et al., 1998). Eq. 5d, derived herein, provides the correct solution for calculating R_j using the $-\Delta I_2$ method. It follows that, if one desires to use the Kirchoff's law expressions for I_j in conjunction with Eq. 2c to calculate R_j, the correct expressions are

$$I_j = I_1 + \frac{V_{m1} - E_{rest1}}{R_{in1}} \tag{1l}$$

and

$$I_j = -I_2 + \frac{V_{m2} - E_{rest2}}{R_{in2}}. \tag{1m}$$

These equations still depend on the precise calculation of E_{rest2} and V_{m2} to accurately determine the value of I_{in2}. Because ΔV_{m2} equals $I_j \cdot R_{c2}$ ($\cong I_j \cdot R_{el2}$, Eq. 2d), the difference between V_2 and V_{m2} is typically small. Hence, the I_j–V_j curve will be shifted only by an amount equal to ΔV_{m2}.

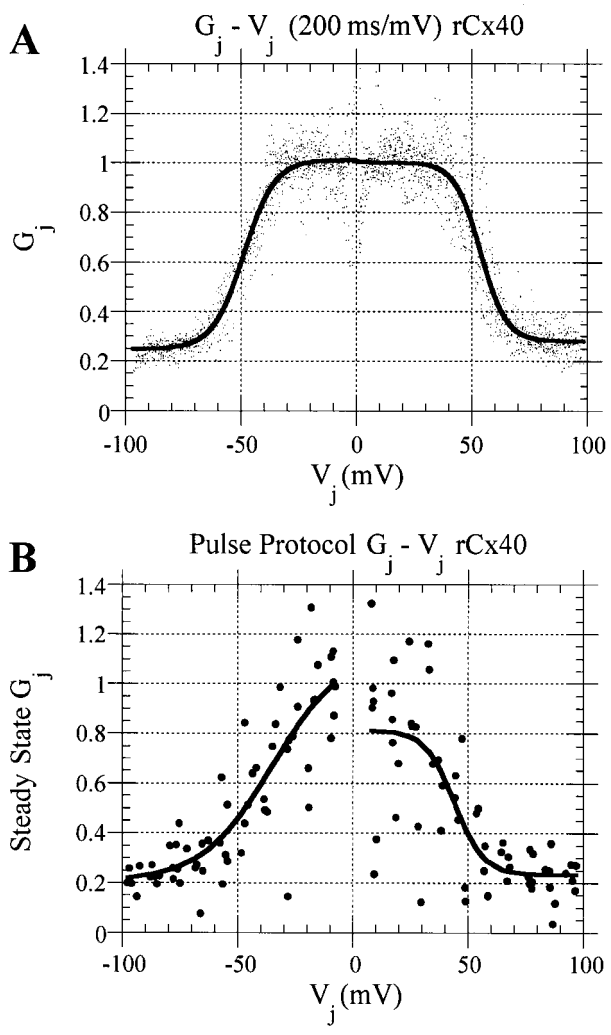

FIGURE 8 Boltzmann distribution of rCx40 steady-state G_j. (*A*) The normalized g_j was calculated for six different rCx40 cell pairs from the I_j–V_j plot divided by the linear slope conductance between ±25 mV. V_j (ΔV_{m1}) was varied by 200 ms/mV from a common holding potential of −40 mV to −140 and +60 mV with a 15-s rest interval between the $-V_j$ and $+V_j$ voltage ramps. Each ramp was repeated five times and the G_j–V_j curve was calculated from the ensemble-averaged I_j–V_j trace. Every data point represents the 20-ms average G_j at a constant V_j (10 points/mV) from each experiment. The solid line is the best fit to the cumulative data points using Eq. 12: $G_j = (G_{max} - G_{min})/[1\text{exp}[zF/RT(V - V_{1/2})]]$. Each half of the G_j–V_j plot was fitted independently, and the Boltzmann parameters are listed in Table 3. (*B*) The same steady-state G_j–V_j curve acquired using a pulse protocol where V_1 was varied in 10-mV increments over a ±100-mV range. The duration of each ΔV_1 pulse and rest interval was 7.5 sec. The values of the fitted parameters for Eq. 12 are listed in the text. The instantaneous g_j was used to normalize the steady-state g_j value of each experiment.

TABLE 3 Boltzmann parameters for steady-state rCx40 G_j–V_j plots

	Beblo et al., 1995		Ramps	
Parameter	$-V_j$	$+V_j$	$-V_j$	$+V_j$
G_{max}	1*	1*	1.00	1.01
G_{min}	0.33	0.28	0.25	0.28
$V_{1/2}$	−54 mV	+47 mV	−49	+54
z	3.2	2.8	−3.7	4.6

*G_{max} was fixed to a value of 1.0 for the Boltzmann fits in Beblo et al., 1995.

The percentage improvement in the R_j estimates for Eq. 2c/1m over Eq. 2c/1k or Eq. 5a is also only 1 or 2 times the percentage value of R_{el2} relative to R_{in2}. As was shown for Eqs. 1f and 1i, the behavior of the two expressions will be similar because the only difference is in the initial estimate of I_{in2}. The data in Figs. 2, 3, and 6 indicate that the $-\Delta I_2$ method (Eq. 5d) is inherently more stable, easier to apply, and frequently more accurate than the Kirchoff's law expression.

Both Eqs. 5a and 5b require knowing the value of R_{el} to make any corrections. The occasional experimenter can accurately account for the error in the R_j estimate by remembering that the actual resistance being measured in the dual whole-cell voltage clamp experiment is $R_{el1} + R_j + R_{el2}$. It follows that the proportion of the command V_j actually applied to the junction is

$$V_j = [(V_1 - V_2) \cdot R_j]/(R_{el1} + R_j + R_{el2}). \quad (2f)$$

The direct measurement of I_j by one whole-cell electrode combined with this corrected V_j value will accurately estimate R_j. It is most convenient to use the cell where V is held constant because I_{in} will not change dramatically, provided that R_{in} remains stable. Contrary to Eq. 1 and 2 from Van Rijen et al. (1998), it is important to keep the same point of reference when alternatively varying V_1 and V_2 to produce a defined V_j. A $-\Delta V$ pulse produces a negative V_1 relative to V_2 when applied to cell 1 but a positive V_1 relative to V_2 when $-\Delta V$ is applied to cell 2. Hence, the net voltage gradient across the gap junction will be oppositely directed whenever the same ΔV is applied alternately to cells 1 and 2. This is especially important when bilateral symmetry is not maintained across the junction, because the resulting E_{rev} or rectifying I_j (and g_j) must maintain the same polarity whether V_1 or V_2 is varied to produce V_j (Barrio et al., 1991; Bukauskas et al., 1995; Suchyna et al., 1999). Figures 5 and 6 illustrate this point in relation to the V_j-gating of rCx40 gap junctions. The −100-mV ΔV step was applied alternately to cells 1 and 2 (traces 2 and 3) and resulted in I_j transients of opposite V_j values.

Because $V_j = [V_1 - (I_1 \cdot R_{el1}) - V_2 + (I_2 \cdot R_{el2})]$ (Eq. 2c), whenever time-dependent changes in I_j occur, the applied V_j will not remain constant. Any asymmetry in $I \cdot R_{el}$ will produce differences in the applied V_j during a ΔV pulse that result in an asymmetric G_j–V_j curve if the command V_j value is used in the final analysis. Because R_j increases as I_j decreases during a constant ΔV, a time-dependent increase in the actual applied V_j also develops. Hence, V_j is not constant during an instantaneous ΔV step and exponential

fits of the decay phase of I_j can result in variable kinetic time constants (τ). The best correction for this variability is to calculate V_j and I_j using correction formulas 2c and 1j (or 1m) for every digitized point. However, variations in V_j still depend on the proportion of the initial voltage drop (i.e., R_{el}/R_j) across the electrode, and kinetic variability will still exist even with the corrections. The operative factor here is $\partial V_j/\partial t$ that may account for some of the kinetic variations in τ_{V_j} (Veenstra, 1991b; Wilders and Jongsma, 1992; Wang et al., 1992; Chanson et al., 1993). A method for determining the equilibrium properties of the steady state G_j–V_j curve devoid of instantaneous fluctuations in V_j was developed. The results of the continuous V_j ramps are reported herein.

Any time there is an asymmetry across the gap junction, a finite voltage will exist across R_j. This will produce a small I_j even when $V_1 = V_2$. It does not matter if the source of the asymmetry is a heterotypic gap junction, asymmetric bilateral ionic salt gradients, or asymmetries in the two whole-cell circuits, $V_j \neq 0$ mV. According to the $-\Delta I_2$ method, this residual I_j will be subtracted out with the $-I_2$ ($V_1 = V_2$) baseline. Hence, small errors can occur using the $-\Delta I_2$ method anytime there is an initial I_j component when $V_1 = V_2$ (Eq. 1g and 5b). The alternative expressions derived from Kirchoff's law offer an improvement over this condition, provided that E_{rest2} is included in the calculation of I_{in2} as presented in Eq. 1i and 5a. For the sake of accuracy, the correct expressions are Eq. 1m and Eq. 2c/1m for the I_j and R_j calculations using the Kirchoff's law expressions. This was demonstrated in Fig. 2, *A* and *B* where the percent error in the R_j estimate was slightly lower at high R_j values ($R_j \geq 2$ GΩ). However, most often when $R_j \geq 2$ GΩ, single-gap junction channel currents are visible in the I_j recording and single-channel analysis methods are used. When single-channel current amplitudes (i_j) are measured from macroscopic I_j traces, this difference between Eqs. 1g and 1i is alleviated. The merits of all-points ("real-time") current histograms also ensure that i_j and I_j are represented as they appeared in the originating whole-cell current recording (Veenstra and Brink, 1992). Under single-channel recording conditions, R_{el} rarely exceeds 1% of R_j or R_{in} and the series resistance errors are minimized. Furthermore, the discrepancies between V_{m1} and V_{m2} when $V_1 = V_2$ rarely exceed 1 mV under adequate dual whole-cell voltage clamp conditions. This fact is demonstrated in Figs. 5 and 6, where actual I_j recordings from homotypic rCx40 gap junctions under symmetrical ionic conditions produced lower *x*-intercept (<1 mV) values with Eqs. 1g and 1j than with Eqs. 1f, 1i, or 1m in 75% of the experiments. The one exception was an experiment where $R_{in1} < 1$ GΩ and the *x*-intercept was 2–3 mV from the origin using Eq. 1g compared to 0.9–1.4 mV with Eq. 1i for the corresponding I_j–V_j curves. In actual application, Eq. 1g (the $-\Delta I_2$ method, Veenstra and Brink, 1992) is more accurate than Eq. 1i (derived from Eq. 1f(A9) in Van Rijen et al., 1998) in estimating I_j from $-I_2$.

Another approach to study the regulation of g_j was to expose the gap junction by shunting R_{in2} and then perfuse with intracellular ions that may modulate cellular function such as H^+, Ca^{++}, Mg^{++}, and ATP^{4-} (Noma and Tsuboi, 1987; Sugiura et al., 1990). The derivations for the "open-cell" configuration (Eqs. 9–11) reveal that it is necessary to determine the value of R_j and R_{in1} prior to establishing this configuration ($R_{oc} = R_j \| R_{in}$) from the dual whole-cell configuration to be quantitatively accurate. Because the open-cell R_j estimate is equally sensitive to R_{in1}, the accuracy of all open-cell R_j measurements are favored by a low R_j/R_{in} ratio. Therefore, this approach is amenable to R_j measurements only when the experimental variable to be tested does not equally affect R_{in}. The primary advantage of this approach is the ability to internally perfuse a gap junction with a variety of ionic solutions in a reversible manner.

The ability to obtain accurate R_j measurements were advanced by the use of V_j ramps to the measure of steady-state V_j-dependent gating (Figs. 7 and 8). V_j was symmetrically increased from 0 to ±100 mV in 1-mV increments of varying duration. Ensemble averages of five V_j ramps of equal duration were normalized to the slope g_j of the I_j–V_j curve from 5–6 different rCx40 cell pairs. The G_j–V_j curves of all experiments were pooled together and fitted with a Boltzmann function (Eq. 12) to estimate the half-inactivation voltage ($V_{1/2}$) and gating charge valence (z) for the V_j-gating of rCx40. G_{max} was within 1% of the normalized value of 1.00, and G_{min} was 0.24 ± 0.04 for all ramp durations tested. These values were in close agreement with previous results using 10-mV, 6-s duration V_j steps (Table 3; Beblo et al., 1995). The slightly lower G_{min} may result from the calculation of actual V_j using Eq. 2c in the g_j calculations or from the 200-ms/mV continuous variation of V_j (20 sec per 100 mV ramp). The new data indicate that the $V_{1/2}$ and z values are similar for $g_j = 2$–7-nS cell pairs when corrected. The largest variations in the actual G_j–V_j curves result from the two experiments where $g_j < 1$ nS because individual channel openings and closings accounted for a larger percent of I_j. The previous G_{max}, G_{min}, and $V_{1/2}$ values were within 2–5% of the values obtained here using V_j ramps and all-points I_j and V_j correction methods. The net gating charge valence (z) increased from 3 to 4 with the continuous steady-state G_j–V_j curve. The continuous I_j, V_j, and g_j analysis provided by the V_j ramps allowed for more accurate fitted curves from fewer experiments as evidenced by the lower standard deviation of the fitted parameters relative to the same results obtained with a pulse protocol. Each experiment also required less time to acquire a single steady-state I_j–V_j curve. This method should be useful to all experimental applications where equilibrium constants are to be determined for an I_j blocking reaction.

In addition to the confirmation of the V_j-gating parameters of rCx40, the rate at which $V_{1/2}$ and z varied with V_j were obtained for the first time. The $V_{1/2}$ decreased from approximately ±70 mV for the 5-ms/mV ramp to a final

value of approximately ±50 mV with a τ of 20–40 ms (Fig. 7). According to the Boltzmann model, $\tau = 1/(\alpha + \beta)$, the opening, α, and closing, β, rates for the gap junction channels (assuming only two states) and $\alpha = \beta$ at $V_{1/2}$ (Harris et al., 1981; Spray et al., 1981). This means that the equilibrium between α and β has a time constant of ≥20 ms, and the opening and closing reaction rates at this V_j are ≤0.1 per ms. The gating charge increased from an initial valence of approximately 2 to a final value of approximately 4 with a τ of ≈100 ms. Most importantly, these data indicate that a gating charge movement with a net valence of 2 occurred as quickly as the settling time of the dual whole-cell voltage clamp circuit. Two additional charges moved in a time- and voltage-dependent manner. This result favors a two-domain V_j-gating mechanism, where one half of the charge lies within the V_j field (membrane) and one-half moves in and out of the V_j field in a time-dependent manner. This is consistent with a proposed mechanism for Cx26 and Cx32, where amino acid residues near the cytoplasmic amino-terminus and the first extracellular loop of the connexins control the polarity of the V_j-gating mechanism (Verselis et al., 1994). Recent evidence further indicates that only a single subunit is required to inactivate the connexin hemichannel, and that the NH_2 terminus lies within the V_j field and undergoes local conformational changes (Oh et al., 2000). The new ramp V_j-gating data provides additional kinetic information that may further identify the mechanism for V_j-dependent gating of connexin channels in a manner analogous to N-type ("ball-and-chain") inactivation of delayed rectifier K^+ channels (Hoshi et al., 1990).

In summary, corrections for I_j and V_j can accurately account for series resistance errors in R_j and g_j estimates in the dual whole-cell patch clamp configuration. Nonzero values for cellular resting potentials (E_{rest}) and junctional potentials (E_{rev}) are also considered and found to be especially important at high R_j values. The quality of the voltage clamp improves during V_j-gating in a time-dependent manner. The alternative open-cell recording configuration requires quantitative assessment of R_{in1} prior to shunting R_{in2} and accuracy is improved if $R_j \ll R_{in1}$. V_j ramps accurately reproduce steady-state g_j properties and provide the advantage of producing a continuous I_j–V_j curve in equal or less time than a conventional pulse protocol. Varying the speed of the V_j ramp can also assess the time-dependence of the net gating charge movement (z) and equilibrium voltage ($V_{1/2}$) at the expense of determining the voltage- and time-dependence of the individual rate constants (α and β).

REFERENCES

Barrio, L. C., T. M. Suchyna, T. Bargiello, L. X. Xu, R. S. Roginski, M. V. L. Bennett, and B. J. Nicholson. 1991. Gap junctions formed by connexins 26 and 32 alone and in combination are differently affected by applied voltage. *Proc. Natl. Acad. Sci. U.S.A.* 88:8410–8414.

Beblo, D. A., H.-Z. Wang, E. C. Beyer, E. M. Westphale, and R. D. Veenstra. 1995. Unique conductance, gating, and selective permeability properties of gap junction channels formed by connexin40. *Circ. Res.* 77:813–822.

Bukauskas, F. F., C. Elfgang, K. Willecke, and R. Weingart. 1995. Heterotypic gap junction channels (connexin26-connexin32) violate the paradigm of unitary conductance. *Pflügers Arch. Eur. J. Physiol.* 429: 870–872.

Chanson, M., K. J. Chandross, M. B. Rook, J. A. Kessler, and D. C. Spray. 1993. Gating characteristics of a steeply voltage-dependent gap junction channel in rat Schwann cells. *J. Gen. Physiol.* 102:925–946.

Hamill, O. P., A. Marty, E. Neher, B. Sakmann, F. J. Sigworth. 1981. Improved patch-clamp techniques for high-resolution current recording from cells and cell-free membrane patches. *Pflügers Arch.* 391:85–100.

Harris, A. L., D. C. Spray, and M. V. L. Bennett. 1981. Kinetics of a voltage-dependent junctional conductance. *J. Gen. Physiol.* 77:95–117.

Hoshi, T., W. N. Zagotta, and R. W. Aldrich. 1990. Biophysical and molecular mechanisms of *Shaker* potassium channel inactivation. *Science.* 250:533–538.

Kolb, H.-A., and R. Somogyi. 1991. Biochemical and biophysical analysis of cell-to-cell channels and regulation of gap junction permeability. *Rev. Physiol. Biochem. Pharmacol.* 118:1–47.

Mazet, F., B. A. Wittenberg, and D. C. Spray. 1985. Fate of intercellular junctions in isolated adult rat cardiac cells. *Circ. Res.* 56:195–204.

Neyton, J., and A. Trautmann. 1985. Single-channel currents of an intercellular junction. *Nature.* 317:331–335.

Noma, A., and N. Tsuboi. 1987. Dependence of junctional conductance on proton, calcium, and magnesium ions in cardiac paired cells of guinea-pig. *J. Physiol. (Lond.).* 382:193–211.

Oh, S., C. K. Abrams, V. K. Verselis, and T. Bargiello. 2000. Stoichiometry of transjunctional voltage-gating polarity reversal by a negative charge substitution in the amino-terminus of a connexin32 chimera. *J. Gen. Physiol.* 116:13–31.

Rook, M. B., H. J. Jongsma, and A. C. G. Van Ginneken. 1988. Properties of single gap junctional channels between isolated neonatal rat heart cells. *Am. J. Physiol. Heart Circ. Physiol.* 255:H770–H782.

Sakmann, B., and E. Neher. 1995. Single Channel Recording, 2nd edition. Plenum Press, NY. 35, 676–677.

Spray, D. C., A. L. Harris, and M. V. L. Bennett. 1981. Equilibrium properties of a voltage-dependent junctional conductance. *J. Gen. Physiol.* 77:77–93.

Suchyna, T. M., J. M. Nitsche, M. Chilton, A. L. Harris, R. D. Veenstra, and B. J. Nicholson. 1999. Different ionic selectivities for connexins 26 and 32 produce rectifying gap junction channels. *Biophys. J.* 77: 2968–2987.

Sugiura, H., J. Toyama, N. Tsuboi, K. Kamiya, and I. Kodama. 1990. ATP directly affects junctional conductance between paired myocytes isolated from guinea pig heart. *Circ. Res.* 66:1095–1102.

Van Rijen, H. V. M., R. Wilders, A. C. G. Van Ginneken, and H. J. Jongsma. 1998. Quantitative analysis of dual whole-cell voltage-clamp determination of gap junctional conductance. *Pflügers Arch.* 436: 141–151.

Veenstra, R. D. 1991a. Physiological modulation of cardiac gap junction channels. *J. Cardiovasc. Electrophys.* 2:168–189.

Veenstra, R. D. 1991b. Developmental changes in regulation of embryonic chick heart gap junctions. *J. Membr. Biol.* 119:253–265.

Veenstra, R. D. 1996. Size and selectivity of gap junction channels formed from different connexins. *J. Bioenerg. Biomembr.* 28:327–337.

Veenstra, R. D., and P. R. Brink. 1992. Patch-clamp analysis of gap junctional currents. *In* Cell–Cell Interactions: A Practical Approach. B. R. Stevenson, W. J. Gallin, and D. L. Paul, editors. IRL Press, Oxford, New York, Tokyo. 167–201.

Veenstra, R. D., and R. L. DeHaan. 1986. Measurement of single channel currents from cardiac gap junctions. *Science.* 233:972–974.

Veenstra, R. D., H.-Z. Wang, E. M. Westphale, and E. C. Beyer. 1992. Multiple connexins confer distinct regulatory and conductance properties of gap junctions in developing heart. *Circ. Res.* 71:1277–1283.

Verselis, V. K., C. S. Ginter, and T. A. Bargiello. 1994. Opposite voltage gating polarities of two closely related connexins. *Nature.* 368:348–351.

Wang, H.-Z., J. Li, L. F. Lemanski, and R. D. Veenstra. 1992. Gating of mammalian cardiac gap junction channels by transjunctional voltage. *Biophys. J.* 63:139–151.

Weingart, R. 1986. Electrical properties of the nexal membrane studied in rat ventricular cell pairs. *J. Physiol. (Lond.).* 370:267–284.

Wilders, R., and H.-J. Jongsma. 1992. Limitations of the dual voltage clamp method in assaying conductance and kinetics of gap junction channels. *Biophys. J.* 63:942–953.

Zhang, Y., D. W. McBride, and O. P. Hamill. 1998. The ion selectivity of a membrane conductance inactivated by extracellular calcium in *Xenopus* oocytes. *J. Physiol. (Lond.).* 508:763–776.

Zhou, X.-W., A. Pfahnl, R. Werner, A. Hudder, A. Llanes, A. Luebke, and G. Dahl. 1997. Identification of a pore lining segment in gap junction hemichannels. *Biophys. J.* 72:1946–1953.